

Objective crystallographic symmetry classifications of noisy and noise-free 2D periodic patterns with strong Fedorov type pseudosymmetries

Peter Moeck

Abstract: Statistically sound crystallographic symmetry classifications are obtained with information theory based methods in the presence of approximately Gaussian distributed noise. A set of three synthetic images with very strong Fedorov type pseudosymmetries and varying amounts of noise serve as examples. The correct distinctions between genuine symmetries and their Fedorov type pseudosymmetry counterparts failed only for the noisiest image of the series where an inconsistent combination of plane symmetry group and projected Laue class was obtained. Contrary to traditional crystallographic symmetry classifications with an image processing program such as CRISP, the classification process does not need to be supervised by a human being. This enables crystallographic symmetry classification of digital images that are more or less periodic in two dimensions (2D) as recorded with sufficient spatial resolution from a wide range of samples with different types of scanning probe microscopes. Alternatives to the employed objective classification methods as proposed by members of the computational symmetry community and machine learning proponents are briefly discussed in an appendix and are found to be wanting because they ignore Fedorov type pseudosymmetries completely. The information theory based methods are more accurate than visual classifications at first sight by most human experts.

I. INTRODUCTION AND BACKGROUND

The symmetries of the Euclidian plane that are compatible with translation periodicity in two dimensions (2D) are tabulated exhaustively in volume A of the International Tables for Crystallography [1] and in the brief teaching edition [2] of that series of authoritative reference books from the International Union of Crystallography (IUCr). Quasicrystalline symmetries are discussed in [3]. Noncrystallographic symmetry has been defined in the on-line dictionary of the IUCr as a “*symmetry operation that is not compatible with the periodicity of a crystal pattern*” [4].

It is also noted in [4] and [5] that this term is often improperly used in biological crystallography, where one should refer either to local and partial symmetry operations on the one hand, and pseudosymmetries, on the other hand. The above mentioned on-line directory defines crystallographic pseudosymmetry simply as featuring a “*deviation*” from a space group symmetry (of one, two and three dimensions) in a crystal space that “*is limited*”

[6], without giving an explanation on how the deviation is to be quantified. In this paper, we will provide such quantifications for three synthetic images.

Pseudosymmetry is “*a spatial arrangement that feigns symmetry without fulfilling it*” [7] and can exist at either the site/point symmetry level of a plane symmetry group or the projected Bravais lattice type level, or a combination thereof. When a very strong translational pseudosymmetry results in metric tensor components that are within experimental error bars indistinguishable from those of a higher symmetric Bravais lattice type, one speaks of a metric specialization [8]. On the site/point symmetry level, one can make a distinction between crystallographic pseudosymmetries that are either compatible with the Bravais lattice of the unit cell of the genuine symmetries or a sublattice of the genuine symmetries. These two pseudosymmetries are often collectively called Fedorov type pseudosymmetries [9]. It is also possible that the pseudosymmetries are incompatible with either of these two lattices.

In the presence of noise, it becomes for human classifiers of crystallographic patterns particularly difficult to distinguish Fedorov type pseudosymmetries that are compatible with the Bravais lattice of the genuine symmetries from their genuine symmetries counterparts. The somewhat less difficult distinction of Fedorov type pseudosymmetries that are compatible with a sublattice of the underlying Bravais lattice from the genuine symmetries has been demonstrated already by this author in a very short conference paper [10]. In that case, a very simple crystallographic pattern was used to which moderate and large amounts of noise were added. It is now time to demonstrate such distinctions for the more difficult problem in this paper.

Pseudosymmetries of the Fedorov type always form their own plane “pseudosymmetry groups”, which are either disjoint or non-disjoint from the plane symmetry group of the genuine symmetries. The lowest symmetric pseudosymmetry groups will (per definition) always be disjoint from the genuine symmetries, but their minimal supergroups can be non-disjoint from the genuine symmetry group. Also per definition, the plane symmetry group of the genuine symmetries is the one that is least broken by the generalized noise in the pattern.

Generalized noise [7] is defined in this paper as the sum of all deviations from the genuine translation periodic symmetries in a crystal’s structure and/or the imaged 2D periodic properties of the crystal. At the experimental level, generalized noise as defined here combines all effects of a less-than-perfect imaging of a crystal, all rounding errors and effects of approximations in the

Peter Moeck is with the Nano-Crystallography Group, Department of Physics, Portland State University, Portland, OR 97207-0751, phone: 503-725-4227; fax: 503-725-2815; e-mail: pmoeck@pdx.edu.

applied image processing algorithms, effects such as uneven staining in the cryo-electron microscopy [11] of intrinsic membrane proteins, and the real structure that typically exist in addition to the ideal structure of a crystal.

Note that it is always only the ideal structure of a crystal that is strictly 2D periodic, but the symmetry group of the ideal structure is per definition the one that the real crystal possesses on average over larger sample regions which feature only a few symmetry breaking structural defects.

Fedorov type pseudosymmetry groups are by these definitions broken to a measurably larger extent than the symmetry group of the genuine symmetries (and all maximal subgroups of these symmetries and their respective maximal subgroups, if those were to exist). This will be further elaborated on in the second section of his paper, where a visual example is provided.

The essence of crystallographic image processing is the enforcing of the site/point symmetries that correspond to a correctly identified plane symmetry group on all of the pixels within the translation averaged unit cell. This is done after translation averaging by symmetrizing the structure-bearing complex Fourier coefficients of the intensity of the more or less 2D periodic image that is to be processed.

When done correctly, crystallographic image processing [12-19] increases the signal to noise ratio of a digital image significantly by means of spatial averaging over all asymmetric units of all unit cells of the selected image area. This enforces all site/point symmetries of a plane symmetry group onto the translation-averaged unit cell. The precondition for correctly processing an image crystallographically is the knowledge of the most likely plane symmetry that a hypothetical version of that image would possess in the absence of generalized noise. For an unknown crystal, this knowledge has historically not been easy to come by and elucidating that kind of plane symmetry group has been a long-standing problem in both the computational symmetry subfield of computer science [20-22] and electron crystallography [11-19].

One of the reasons that this problem had remained unsolved for more than half a century are inclusion relations between crystallographic symmetry groups, classes, and types [1,2]. In other words, one of the reasons was non-disjointness of many of the geometric models that are to be compared to the input image data and from which the best, i.e. statistically most justified, model is to be selected. Symmetry inclusion relations, non-disjointness and disjointness are explained in some detail in the third section of this paper. That section also presents the plane symmetry hierarchy tree as a visualization of disjoint and non-disjoint symmetry inclusion relationships between the translationengleiche [1,2] maximal subgroups and minimal supergroups of the plane symmetry groups.

This author presented recently a so far unique threshold-free solution to identifying the genuine plane symmetry group in a digital more or less 2D periodic image in the presence of pseudosymmetries and generalized noise [7,10,23,24]. Fedorov type pseudosymmetries do not present challenges to this solution as they are reliably identified (and can be quantified) as long as noise levels are moderate. This will be demonstrated in this paper.

The author's solution is based on Kenichi Kanatani's geometric form of information theory [25-27] and complemented by analogous methods to identify the projected Laue class [7,10] of such an image as well as its projected Bravais lattice type [28]. Kanatani's theory presents a geometric "workaround" to the inclusion relations problem and has the added benefit that the prevailing noise level does not need to be estimated for the comparison of non-disjoint geometric models of digital image data. This theory tackles the inclusion problem that a less restricted, e.g. lower symmetric, model of some input image data will always feature a smaller deviation (by any kind of distance measure) to the input image data than any more restricted, e.g. higher symmetric, model that is non-disjoint. In other words, the fit to some experimental data with more parameters will always be better than a fit with fewer parameters.

The third section of this paper gives the relevant equations and inequalities for making objective plane symmetry and projected Laue class classifications with the author's methods so that they can be used in the fourth section. Objectivity is in this paper to be understood as only stating what the image data actually reveal about a crystallographic symmetry without any subjective interpretation of any symmetry distance measure.

Note that information theory based crystallographic symmetry classification methods should also be developed for crystallographic symmetry classifications in three spatial dimensions because there is also subjectivity in the current practice of single crystal X-ray and neutron crystallography [7].

When the underlying plane symmetry in a noisy experimental image has been underestimated, i.e. only a subgroup of the most likely plane symmetry group has been identified, one does not make the most out of the available image data in the subsequent symmetry enforcing step in the crystallographic image processing. On the other hand, if the plane symmetry is overestimated, "non-information" due to noise will unavoidably be averaged with genuine structural information in the subsequent processing (symmetry enforcing) of the image.

In the latter case, one may have wrongly identified a minimal supergroup of the correct plane symmetry group that the analyzed image would possess in the absence of generalized noise. That supergroup would be the union of the genuine (least broken) plane symmetry group and one (or more) Fedorov type pseudosymmetry group(s).

It is, accordingly, very important to get the crystallographic symmetry classification step of the crystallographic image processing procedure just right. For that, one should only rely on the digital image data itself and refrain from any subjective considerations. The inclusion of prior knowledge into such considerations would be fine if done at a formal mathematical level.

Common practice in electron crystallography is so far, however, to make such considerations based on residuals between the translation averaged image and differently symmetrized versions of it that are based on the structure-bearing Fourier coefficients of the image intensity [11-19]. It has recently been noted with respect to cryo-electron microscopy that "... as currently practiced, the procedure

is not sufficiently standardized: a number of different variables (e.g. ... threshold value for interpretation) can substantially impact the outcome. As a result, different expert practitioners can arrive at different resolution estimates for the same level of map details.” [11].

With the author’s objective and interpretation-threshold-free methods [7,10,23,24], one can now make advances with respect to the stated situation in the cryo-electron microscopy [11] subfield that deals with intrinsic membrane proteins, in the electron crystallography of inorganic materials, and in the crystallographic processing of digital images in general.

It is a very well known that the spatial resolution of crystallographic studies depends on the number of structural entities over which one averages [29]. The correct averaging can, however, only be obtained for the correct prior symmetry classification of the data that enter into such studies when no prior knowledge of the plane symmetry is available. In crystallographic image processing on the basis of the correctly identified plane symmetry group, one enforces all of the site/point symmetries that the translation averaged unit cell image need to feature in order to be the best representation of the input image data in the information theoretic sense. This is often called the “Kullback-Leibler best” (or simply K-L best) geometric model that the input image data maximally supports.

Compared to standard Fourier filtering [30], the processing of a digital image in the correctly determined plane symmetry group leads to a further increase of the signal to noise ratio and an associated increase of the spatial resolution of a crystallographic study. For approximately Gaussian distributed noise, crystallographic image processing is by the square root of the multiplicity of the general position per lattice point (equal to the number of non-translational symmetry operations in the group) more effective in the suppression of noise than Fourier filtering alone.

Two different sets of Fourier coefficient based residuals, as implemented in the crystallographic image processing programs CRISP [13-15] and ALLSPACE [11], are most popular in the electron crystallography community.

Neither of these two sets of residuals are maximal likelihood estimates combined with a geometric bias correction term for objective symmetry model selection of the image data. A geometric form of information theory can not, therefore, be based on these residuals in order to avoid a necessarily subjective decision of what the underlying plane symmetry most likely is (in the considerate opinion of the users of these two programs).

The sets of typically employed residuals in electron crystallography quantify deviations of the experimental image with respect to differently symmetrized versions of it, but the decision which plane symmetry group is to be enforced on the image data as part of its crystallographic image processing is with necessity left to the electron crystallographer. The CRISP program will make a suggestion that the user may either accept or overwrite, but relies heavily on visual comparisons between differently symmetrized versions of the input image data.

This author has not used ALLSPACE (in its 2dx incarnation [16]) so far as no version that runs on Microsoft windows compatible computers seem to exist. There are also competing computer programs with less comprehensive residuals, e.g. VEC [20,21] and EDM [22] that rely even more heavily on visual comparisons of the translation averaged image to its fully symmetrized versions. Note that VEC stands for “visual computing in electron crystallography” and is very aptly named with respect to its reference to a human being’s vision.

The benefits of the correct crystallographic processing of a more or less 2D periodic image will be demonstrated as a secondary goal of this paper. Scanning probe microscopists should take notice as these demonstrations are mainly directed to them. This is because crystallographic image processing is just as applicable to more or less 2D periodic images from scanning probe microscopes [24,28] as it is to images from parallel illumination transmission electron microscopes (as used in electron crystallography). Scanning probe microscopists may, however, like to correct for systematic scanning distortions in their images of more or less 2D periodic samples with a tool such as Smart Align [31] before they make crystallographic symmetry classifications and process their images crystallographically.

The main goal of this paper is to demonstrate the author’s threshold-free classification methods on a series of three synthetic images. This should help winning over the computational symmetry, electron crystallography, and scanning probe microscopy communities to replace their subjectivity in crystallographic symmetry classifications with the objectivity that the information theory based methodology enables.

The limiting effects of noise and Fedorov type pseudosymmetries in more or less 2D periodic images on crystallographic symmetry classifications have so far rarely been analyzed. As one would expect, the distinction between genuine symmetries and pseudosymmetries of the Fedorov type becomes more difficult with increasing amounts of noise even when a geometric form of information theory is used [10]. This will be demonstrated here once more, but in much more detail, in the fourth section this paper. That section constitutes this paper’s main part and features three subsections containing nine numerical data tables as well as four figures. One of these figures demonstrates both the beneficial noise reduction and spatial resolution enhancement effects of crystallographic image processing and some of its rather minor artifacts.

In order to facilitate direct comparisons to results obtained by one of the two most popular traditional crystallographic symmetry classification methods of electron crystallography [13-15], *.hka files were exported from CRISP and used for the calculation of the ratios of sums of squared residuals (as parts of minimized geometric Akaike Information Criterion (G-AIC) values) of non-disjoint and disjoint geometric models for the image input data. Note that CRISP does not provide a direct estimate of the point symmetry in the amplitude map of a discrete Fourier transform, which is here referred to as

the projected Laue class of a more or less 2D periodic image.

The fifth section of this paper compares the results of our three crystallographic symmetry classifications (by the author's information theory based methods) to plane symmetry group estimates by the program CRISP as applied to the same and adjacent images areas of the three synthetic images. The paper ends with a summary, conclusions, and outlook section.

The first appendix presents the hierarchy tree graph of the crystallographic 2D point groups that are projected Laue classes. The second appendix gives the equations for the calculation of ad hoc defined confidence levels for crystallographic symmetry classifications by the author's methods into plane symmetry groups and projected Laue classes.

The third appendix briefly discusses crystallographic symmetry classifications by alternative methods. Comments on what has so far been achieved by others with alternative computational symmetry and machine learning approaches are provided there. That discussion extends an earlier review by this author of the whole field of direct and reciprocal/Fourier space based crystallographic symmetry classifications of digital images that are more or less periodic in 2D [32].

II. FEDOROV TYPE PSEUDOSYMMETRIES ILLUSTRATED ON A NOISE-FREE SYNTHETIC IMAGE

Figure 1 shows a slightly enlarged reproduction of a crystallographic pattern that originated with the graphic artist Eva Knoll [33]. After expansion by periodic motif stitching of a digital representation of the original artwork as presented in [33], that pattern features in total approximately 144 primitive unit cells. Only some 25 unit cells are shown in Fig. 1. The computer program Image Composite Editor [34] was used for the periodic motif stitching. There are about 24 periodic motifs in the original artwork, as far as this can be inferred from Knoll's paper.

The digital pattern in Fig. 1 serves in this paper as the basis of three synthetic images that are to be classified with respect to their crystallographic symmetries and Fedorov type pseudosymmetries. The two per design noisy versions of the pattern (in the series of analyzed images) are subsequently processed crystallographically in order to demonstrate the technique's benefits with respect to the noise suppression and site/point symmetry enforcing of such a processing.

Because the physical piece of graphic art from which the digital pattern in Fig. 1 was created is hand made, none of the 2D translation compatible crystallographic symmetries of the Euclidean plane are strictly speaking present (as they are only mathematical abstractions). It is, however, standard practice to assign a plane symmetry group to such a crystal pattern as one would also do for any sufficiently well resolved image from a real crystal in the real world.

That symmetry group is per definition the one that is least broken by structural, sample preparation, imaging, and image processing imperfections (generalized noise). For the purpose of this demonstration, the assumption is made that the imaging and image processing imperfections

in the pattern in Fig. 1 are negligible and that there are no structural imperfections/defects that are intrinsic to the imaged object. The generalized noise in that pattern is, therefore, negligible and we call this image the noise-free member of a series of three images that are to be classified with respect to their crystallographic symmetries and Fedorov type pseudosymmetries in this paper.

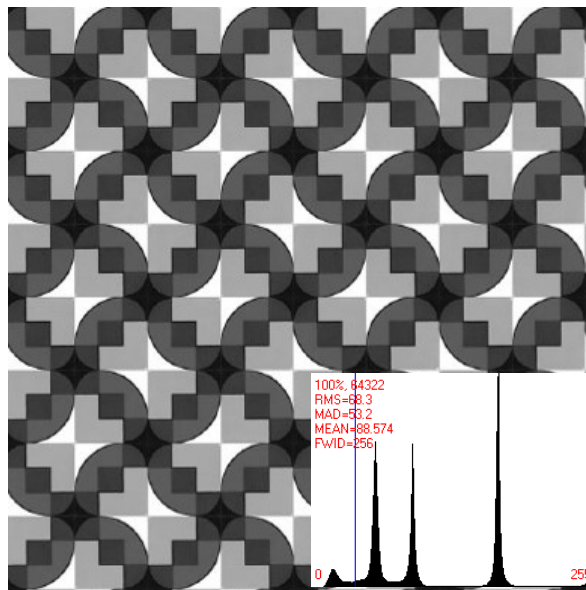


Fig. 1. Reproduction of a digital photo or otherwise digitized version of the graphic artwork “Tiles with quasi-ellipses” (1992, acrylic on ceramic) by Eva Knoll with histogram as inset. The blue thin line and descriptive annotations in red ink in the histogram are due to the program CRISP.

The graphic artist might have had the intention to “amuse” (maybe also somewhat confuse) a human classifier of the art object's crystallographic symmetries by presenting a combination of genuine symmetries and strong pseudosymmetries of the Fedorov type. (If that was indeed one of her objectives, that artist has succeeded in confusing this author for a while.) The approximate translation symmetry of the piece of graphic art is clearly revealed in the crystallographic pattern in Fig. 1. Approximate point/site symmetries in the approximate unit cells can also be recognized visibly.

A human expert classifier would most likely assign plane symmetry group $p4gm$ to the pattern in this image at first sight because approximate four-fold and two-fold rotation points as well as mirror and glide lines are all visibly recognizable in their required spatial arrangements in all of the more or less translation periodic unit cells of the crystallographic pattern in Fig. 1.

The different types of visually recognizable point/site symmetries in all individual unit cells are probably broken by slightly different amounts, but these differences appear to be so minor that a human being may just assume they are all broken by exactly the same amount. Under this assumption, plane symmetry group $p4gm$ would indeed underlie the completely symmetric idealization of the crystallographic pattern in Fig. 1. The rather sharp peaks in the histogram in Fig. 1 are to be interpreted as genuine characteristics of the underlying crystallographic pattern

since no noise was added to deliberately disturb this pattern.

The image-pixel-value based classification of this pattern with the author's method reveals, however, plane symmetry groups $p2$ and $p4$ as genuine, i.e. least broken, and the Fedorov type pseudosymmetry groups $plgl$, $pllg$, $clml$, and $c1lm$ as quantitatively more severely broken than the $p2$ and $p4$ symmetries. These pseudosymmetries combine with the genuine symmetries to the two minimal pseudo-supergroups $p2gg$ and $c2mm$, as well as their respective minimal pseudo-supergroup $p4gm$.

The forth section of this paper gives the details of the corresponding analysis. The point/site symmetry of the centers of the quite conspicuous bright “bow ties” in this pattern is visibly no higher than point symmetry group 2, which is one of the maximal subgroups of $2mm$. Site symmetry $2mm$ is, on the other hand, one of the minimal supergroups of point symmetry group 2, but visibly more severely broken in the crystallographic pattern in Fig. 1.

This becomes even clearer in Figs. 2 and 3. Approximately two unit cells of this pattern are displayed in Fig. 2 after translation averaging by Fourier filtering¹.

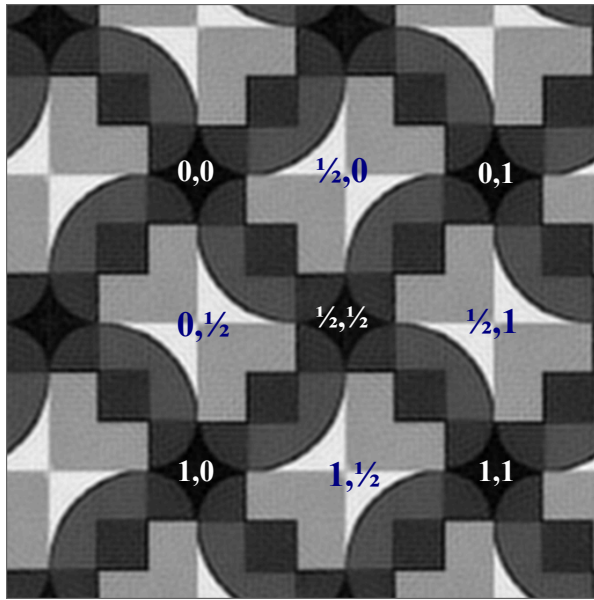


Fig. 2. Approximately two translation averaged unit cells of the pattern in Fig. 1 after Fourier filtering over approximately 88 stitched-together primitive unit cells and using 956 structure-bearing Fourier coefficients. Selected fractional unit cell coordinates as insets.

Note that each white bow tie in Fig. 2 is shared between two adjacent unit cells that are based on what seems to be

¹ The obtaining of satisfactory Fourier filtering results was facilitated by the above mentioned increase in the number of unit cells in the crystallographic pattern that underlies Fig. 1 by computational periodic motif stitching. This kind of computational increase of a digital image of the original graphic work of art is also highly beneficial to the subsequent crystallographic symmetry classification and a possible follow up step of the enforcing of the plane symmetry that most likely underlies the pattern in a statistically sound sense. Note also that Fourier filtering [30] is integral part of symmetry classifications and any subsequent crystallographic image processing. This is because the sums of squared residuals and the symmetrizing of the input image data are based only on the periodic structure-bearing Fourier coefficients of a digital image.

square Bravais lattice. The centers of the bright bow ties are at fractional unit cell coordinates $\frac{1}{2}, 0$, $\frac{1}{2}, 1$, $0, \frac{1}{2}$, and $1, \frac{1}{2}$, as marked by insets in Fig. 2. These points feature visually the approximate site symmetry group 2 at best, rather than $2mm$, which would be required if the underlying plane symmetry group were to be $c2mm$ or $p4gm$. The observed site symmetry 2 at these fractional unit cell coordinates is, on the other hand, compatible with plane symmetry groups $p2$, $p2gg$, and $p4$.

At the fractional unit cell coordinates $0, 0$, $1, 0$, $0, 1$, and $1, 1$ as well as $\frac{1}{2}, \frac{1}{2}$ in Fig. 2, there are also clearly visible approximate four-fold rotation points at the centers of very dark “curved diamonds” so that a $p4$ or $p4gm$ classification by a human expert is probably the best anyone could come up with when the slight differences in the breaking of the individual symmetry operations are not noticed and quantified. The genuine plane symmetry group of this image can, however, only be $p2$, $p2gg$, or $p4$ when the visible site/point symmetry around the centers of the white bow ties are taken into account. Section IV will reveal which one of so symmetrized geometric models of the pattern in Fig. 1 is best in the minimal expected Kullback-Leibler divergence sense.

Figure 3 zooms into the translation periodic motif (after translation averaging) and features a single white bow tie and its immediate surrounding. Both of the arrows point to positions in the motif where the tips of the white bow ties end and meet straight lines from the gray L-shaped parts of the motif. There is approximately a 20 % difference in the distance of these points from the horizontal and vertical edges of the gray “right angle ruler” shaped motif parts, so that there is no mirror line from the top-right corner to the bottom left corner in this figure, as would be required for the whole motive to be part of a unit cell with plane symmetry group $p4gm$.

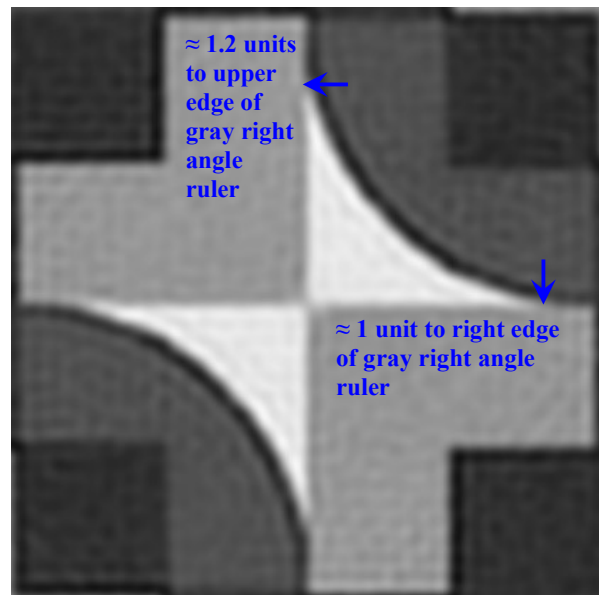


Fig. 3. One white bow tie in a close up. There is probably no longer an argument that the point symmetry of this feature is at best point group 2.

Another example of a visual and analytical discrimination between a genuine plane symmetry group

and Fedorov type pseudosymmetries in a synthetic image has been presented in [10]. The visual difference between the least broken plane symmetry and the Fedorov type pseudosymmetries in the noise-free image is clearly revealed in that short conference paper. That other paper demonstrated also that the author's methods identify the genuine symmetry and pseudosymmetry correctly in the presence of a modest amount of noise, but fail to do so for a large noise level when very small Fourier coefficients are ignored. Some of these structure-bearing Fourier coefficients were weak superlattice reflections that might easily be masked by noise in Fourier space and, therefore, overlooked. Strictly Gaussian distributed noise was used in that other paper [10].

These results were all rather similar to the results of this study as presented in the fourth section of this paper. The main differences here are that the crystallographic symmetry classifications are described in some detail, backed up by data tables, and that much more sophisticated patterns (based on a bona fide graphic artist's work) were analyzed. As another noticeable difference to the analysis in [10], the added noise in the analyzed patterns is in this paper only approximately Gaussian distributed by design.

III. PERTINENT EQUATIONS, INEQUALITIES, AND THE PLANE SYMMETRY HIERARCHY TREE

As mentioned above, the Fourier coefficient residuals of CRISP are not in a form that allows for their usage as part of a G-AIC because they are not maximal likelihood estimates. Kanatani's G-AIC relies on the noise being approximately Gaussian distributed. For that kind of noise, the matching maximal likelihood estimate takes the form of sums of squared residuals between the input data and geometric models for that data.

Since crystallographic symmetry classifications are best done in Fourier space, the maximal likelihood estimates for approximately Gaussian noise in more or less 2D periodic patterns takes the form of the sums of squared residuals of the complex structure-bearing Fourier coefficients for plane symmetry group classifications. For projected Laue class classifications, they take the form of the sums of squared residuals of the amplitudes of those Fourier coefficients.

The residuals are calculated as sums of squared Fourier space differences between the (Fourier) coefficients of the Fourier filtered input image data and the differently symmetrized geometric models for this data. Equation (1) gives the sum of squared residuals of the complex Fourier coefficients of a symmetrized geometric model of the input image data with respect to the translation-averaged-only (Fourier filtered) version of this data:

$$\hat{J}_{cFC} = \sum_{j=1}^N (F_{j,trans} - F_{j,sym}) * (F_{j,trans} - F_{j,sym}) \quad (1),$$

where $(.)^*$ stands for the complex conjugate of the difference of a pair of complex numbers $(.)$. The sum is over the differences of all N structure-bearing Fourier coefficients with matching Laue indices, and the subscripts

on the right hand stand for *translation averaged* and *symmetrized*, respectively. The subscript on the left hand side stands for *complex Fourier coefficients*. Note that there is a zero sum of residuals per equation (1) for the case of $F_{j,trans} = F_{j,sym}$, i.e. the translation-averaged-only geometric model of the input image data, which features plane symmetry group $p1$.

The sum of squared residuals of the amplitudes of the Fourier coefficients is calculated in an analogous way from the real valued amplitudes of the structure-bearing Fourier coefficients:

$$\hat{J}_{aFC} = \sum_{j=1}^N (|F_{j,trans}| - |F_{j,sym}|)^2 \quad (2),$$

where the subscript on the left hand side stands for *amplitude of Fourier coefficients*.

Note again that there is a zero sum of residuals when all of the translation averaged and symmetrized Fourier coefficient amplitudes with matching Laue indices are equal to each other. This happens for the translation-averaged-only geometric model of the input image data, which features point symmetry 2 due to the Fourier transform being centrosymmetric. Projected Laue class 2 features, accordingly, a zero sum of amplitude residuals in the data tables that are show in the fourth section.

In order to restrict the sums of squared residuals to reasonably small numbers, the Fourier coefficients of the input image intensity and their symmetrized versions are normalized by division of the maximal amplitudes that the CRISP program provides for both the translation averaged model and the symmetrized models of the input image data in both equations (1) and (2). (That maximum is set to 10,000 for the translation averaged image data as obtained by CRISP.)

What follows below is valid for classifications into both plane symmetry groups and projected Laue classes. The same equations and inequalities as well as analogous considerations concerning the plane symmetry group hierarchy and the hierarchy of 2D point groups that are Laue classes apply so that the subscripts FC and L on the sums of squared residuals from equations (1) and (2) are dropped below. Two different symmetry hierarchy trees will, however, be applicable. The first one for plane symmetry groups will be presented as Fig. 4 below. The second one for projected Laue classes is given in the first appendix.

Kanatani's G-AIC has the general form:

$$G - AIC(S) = \hat{J} + 2(dN + n)\hat{\varepsilon}^2 + O(\hat{\varepsilon}^4) + \dots \quad (3),$$

where \hat{J} is a sum of squared residuals, as for example given in (1) and (2) for the geometric model S , d is the dimension of S , N is the number of data points that represent the model S , n is the number of degrees of freedom of S , and $\hat{\varepsilon}^2$ is the variance of a generalized noise term, which obeys a Gaussian distribution to a sufficient approximation. The $O(\hat{\varepsilon}^4)$ term in (3) represents unspecified terms that are second order in $\hat{\varepsilon}^2$, while the ellipsis indicates higher-order terms that become progressively smaller.

For crystallographic symmetry classifications of more or less 2D periodic images, the dimension of the geometric model is zero (as it is the intensity value of individual pixels that are considered to be mathematical points). The degrees of freedom of the geometric models in this paper depend on the number of non-translational symmetry operations in the plane symmetry groups to which the translation-averaged input image data has been symmetrized. They are obtained by the ratio

$$n = \frac{N}{k} \quad (4),$$

where k is the above mentioned number of non-translational symmetry operations, which is equal to the multiplicity of the general position per lattice point in all plane symmetry groups.

For small and moderate amounts of generalized noise, it is justified to ignore all of the higher order terms in (3):

$$G - AIC(S) = \bar{J} + 2(dN + n)\hat{\varepsilon}^2 \quad (5).$$

The number of data points N can either be constant for all geometric models or differ from model to model. The dimension of the model is defined by the type of geometric model.

Equation (5) is to be interpreted as a “balanced model residual” for geometric model selections that is well suited to deal with symmetry inclusion relations. A non-disjoint and less-constrained model, which is lower symmetric, will always fit the input data better (assuming N being constant) than the more constrained model that features a higher non-disjoint symmetry. The \bar{J} value of the less constrained (more general) model that is in a non-disjoint relationship with a higher symmetric model will, therefore, be smaller than its counterpart for the more constrained model. In other words, the more general model fits the data better than the more restricted model. This is because the more general (less constraint) model has more parameters.

The geometric model-bias correction term $2(dN + n)\hat{\varepsilon}^2$ in (5) will for the less constrained model be larger than its counterpart for the more constrained model (assuming $k > 1$ and, for convenience, an equal N for both models). In other words, the better fitting, less constrained, model features a higher “model selection penalty” than its worse fitting, more constrained, counterpart. This kind of interplay between fitting the input image data better at the expense of a higher model selection penalty provides the basis for objective geometric model selections by the minimizing of their G-AIC values over a complete set of models.

As long as the G-AIC value of a more constrained, higher symmetric model, subscript m , is smaller than that of the less constrained model, subscript l , the former model is a better representation of the input image data than the latter:

$$G-AIC(S_m) < G-AIC(S_l) \quad (6).$$

The rational geometric model selection strategy is to minimize the G-AIC values (rather than only the sums of squared residuals) for a whole set of geometric models by

means of repeated applications of inequality (6). As there are two models, S_m and S_l in (6), one sets this inequality up for non-disjoint pairs of geometric models, one at a time, and tests if (6) is fulfilled.

This allows for a more constrained/symmetric model of the input image data to be selected in a statistically sound manner as better representation of the input data although its numerical fit, as measured by its sum of squared residuals, is actually less than that of the less constrained/symmetric model. Note that the identification of which of the two geometric models is the better representation of the input image data is based solely on the input data itself and the underlying mathematic [26,27] of Kanatani theory. (In this paper, the mathematics of crystallographic symmetries [1,2] comes obviously into play as well.)

There is no arbitrarily set threshold for the identification of the better model in the presence of a symmetry inclusion relationship, just an inequality that needs to be fulfilled numerically. All of the other crystallographic symmetry classification methods that were so far used in electron crystallography [11-19] and the computational symmetry community [20-22] feature such thresholds.

At first sight, it would seem that estimates of $\hat{\varepsilon}^2$ are needed to make objective geometric model selections by the minimization of their G-AIC values by means of inequality (6) and the definition of the model selection criterion (5). Each geometric model features a different separation of the presumed geometric information amount, on the one hand, and presumed non-information/generalized noise amount, on the other hand.

There is, however, a workaround to estimating $\hat{\varepsilon}^2$ that not only identifies the best possible separation of geometric information and non-information, but also gives an estimate of the prevailing noise in the input image data. The workaround in this paper takes advantage of the translationengleiche [1,2] symmetry inclusion relations between plane symmetry groups as shown in Fig. 4, i.e. non-disjointness in other words. We will explain the workaround for plane symmetry classifications in this section of the paper and refer to the first appendix for specifics that need to be considered in order to use this workaround for projected Laue class classifications.

The number of non-translational symmetry operations, k is one of the two ordering principles of the hierarchy tree of the translationengleiche plane symmetry groups, Fig. 4. The other ordering principle in this figure is the non-disjointness of maximal subgroups and minimal supergroups. These symmetry inclusion relations are in Fig. 4 marked by arrows between maximal subgroups and minimal supergroups.

Translationengleiche in the previous paragraph means that the addition of a non-translational symmetry operation to the unit cell of a lower symmetric group, which has the status of a maximal subgroup, results in the unit cell of a higher symmetric group, which is the former’s minimal supergroup. Changes from a primitive unit cell to a centered unit cell and vice versa are permitted [35] (as they represent essentially orientational changes of symmetry operations with respect to the unit cell vectors).

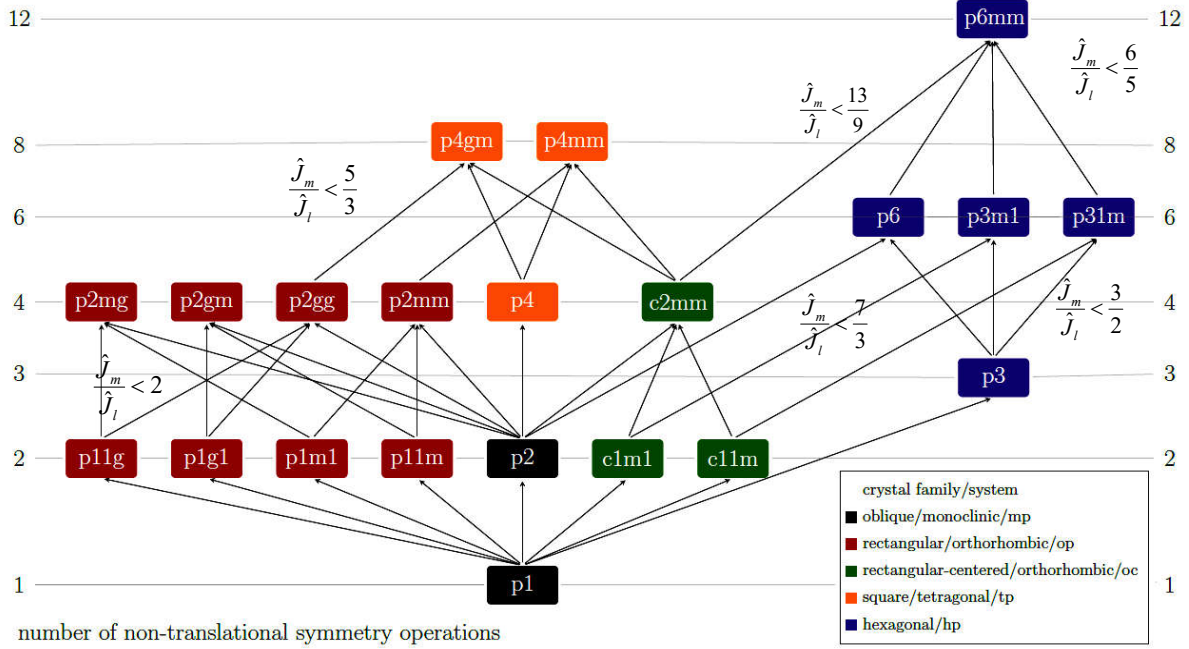


Fig. 4. Hierarchy tree of the translationengleiche plane symmetry groups with ratios of sums of squared complex Fourier coefficient residuals as insets. The inset ratios are valid for equal numbers of structure bearing Fourier coefficients of geometric models and apply to transitions from a k_l level of the graph to a permitted k_m level. Maximal subgroups are connected to their minimal supergroups by arrows.

The translation averaged geometric model of some input image data (with plane symmetry group $p1$) is non-disjoint from the $c1m1$ symmetrized model of these data, as that plane symmetry groups is a minimal supergroup of $p1$. The centered plane symmetry group $c1m1$ with $k = 2$ is in turn in a maximal subgroup relationship with plane symmetry group $p3m1$ with $k = 6$, see Fig. 4.

The number of non-translational symmetry operations in each plane symmetry group, k , is given on both the left and right hand side of Fig. 4 and increases from the bottom to the top of the hierarchy tree. The connecting arrows in Fig. 4 mark plane symmetry groups as being non-disjoint. Whenever there is no arrow connecting two plane symmetry groups in Fig. 4, that pair of groups is disjoint in the translationengleiche sense.

In the above mentioned workaround to estimating $\hat{\epsilon}^2$, one sets up inequality (6) for two non-disjoint models of the input image data that were symmetrized to non-disjoint plane symmetry groups, i.e.

$$\hat{J}_m + 2(dN_m + \frac{N_m}{k_m})\hat{\epsilon}_m^2 < \hat{J}_l + 2(dN_l + \frac{N_l}{k_l})\hat{\epsilon}_l^2 \quad (7),$$

and takes advantage of both the inequality sign and the estimate

$$\hat{\epsilon}_l^2 \approx \frac{\hat{J}_l}{rN_l - n_l} \quad (8),$$

for the amount of approximately Gaussian distributed noise, where r is the co-called co-dimension in Kanatani's framework, which is for our case equal to one².

Because the more symmetric/restricted model, subscript m , that fulfills inequality (7) will provide a better separation of noise/non-information and signal/structural information in the image, we have $\hat{\epsilon}_m < \hat{\epsilon}_l$, so that we can replace $\hat{\epsilon}_m$ with $\hat{\epsilon}_l$ on the left hand side of (7) without changing the fundamental meaning of the inequality. This allows us to recast this inequality into

$$\frac{\hat{J}_m}{\hat{J}_l} < 1 + \frac{2(k_m - \frac{N_m}{N_l}k_l)}{k_m(k_l - 1)} \quad (9a),$$

with $d = 0$.

Note that per inequalities (9a) and (9b), comparisons of all geometric models that have been symmetrized to minimal supergroups of $p1$ to the translation-averaged-only input image data are impossible, as $k_l = 1$ in all of these cases. There is also a zero sum of squared complex Fourier coefficient residuals of $\hat{J}_{l=1}$ in all of these cases, so that there is no inconsistency. One, therefore, simply assumes that there is indeed more than translation symmetry in the input image data and uses these inequalities with $k_l = 2$ and 3 as minimum. After having made that assumption, one proceeds with determining what

² This is because the dimension of the data space is one (intensity values of pixels). The co-dimension is the difference between the dimension of the data space and the dimension of the model space = 0.

symmetry operations there are in the input image data and to what plane symmetry group they combine.

One needs to carefully distinguish between genuine plane symmetry groups and possibly existing pseudosymmetry groups in the input image data based on the model pair's \hat{J}_m , \hat{J}_l , k_m , and k_l . Based on the definitions in the first section of the paper, the least broken symmetry at the $k_l = 2$ and 3 is the first genuine symmetry that is identified and all other genuine symmetries are “anchored” on this particular symmetry group.

For the special case $N_m = N_l$, inequality (9a) reduces to

$$\frac{\hat{J}_m}{\hat{J}_l} < 1 + \frac{2(k_m - k_l)}{k_m(k_l - 1)} \quad (9b),$$

and one can take advantage of the inequality having now the simple form of a numerical value on its right hand side that is just the sum of unity and a constant term that only depends on the difference in the hierarchy levels, k , of the respective two symmetrized non-disjoint models/plane symmetry groups that are to be compared to each other³, see Fig. 4. The respective ratios of sums of squared complex Fourier coefficient residuals are provided in Fig. 4 as insets for easy reference.

Inequality (9b) can be used in connection with ad hoc defined confidence levels for geometric model selections [28]. Providing such confidence levels can be understood as giving a quantitative measure of the corresponding model-selection-uncertainty, which needs to accompany any crystallographic symmetry measurement results in order to be complete [36].

The second appendix gives the formulae for calculating confidence levels for both plane symmetry and Laue class classifications. We will, however, not use inequality (9b) and equations (A-1) to (A-4) in this paper as their precondition $N_m = N_l$ is in general not met in our study. This is due to the usage of as exported *.hka files from the CRISP program or, in other words, due to the set up of this particular study. It is also possible to generalize the confidence level equations by basing them on inequality (9a).

In practice, one begins an objective crystallographic symmetry classification with calculating the sums of squared residuals for all of the geometric models that feature a multiplicity of the general position per lattice point (number of non-translational symmetry operations) of two and three, see Fig. 4. Note that plane symmetry groups $clm1$ and $cllm$ feature two non-translational symmetry operations each, the multiplicity of the general position in the centered unit cell is four, but there are two lattice points per unit cell.

All of the geometric models with two and three non-translational plane symmetry operations are disjoint from each other per definition. Combinations of the groups with two and three non-translational plane symmetry operations lead to the majority of plane symmetry groups that are higher up in the hierarchy tree graph, Fig. 4.

When there is more than translation symmetry in the input image data, at least one of the geometric models that has been symmetrized to a plane symmetry group with two or three non-translational symmetry operations will have a very low sum of squared residuals of the complex Fourier coefficients. The plane symmetry group of that model is necessarily non-disjoint from its minimal supergroups so that tests if a “climbing up” in the plane symmetry hierarchy tree is allowed by inequality (9a) can proceed.

Let us assume for the sake of the argument that the geometric model with the lowest sum of squared residuals was the one that was symmetrized to plane symmetry group $p2$ and Laue class 2. This plane symmetry group features $k_l = 2$ in the plane symmetry hierarchy tree in Fig. 4.

We see that this plane symmetry group is in minimal supergroup relationships with plane symmetry groups $p2mg$, $p2gm$, $p2gg$, $p2mm$, $p4$, and $c2mm$ at the $k_m = 4$ level, as well as with $p6$ at the $k_m = 6$ level, Fig. 4. Let us further assume that the sums of squared residuals for plane symmetry groups $plm1$, $pllm$, $clm1$, and $cllm$ are two to three orders of magnitude larger than for $p2$. This would mean that there are no mirror lines in the input image data and plane symmetry groups that contain mirror lines at the $k_m = 4$ level are to be ruled out as correct classification of the input image data.

Let us further assume that the sums of squared Fourier coefficient residuals for the models that were symmetrized to plane symmetry groups $p4$ and $p6$ are also two to three orders of magnitude larger than that for $p2$. This means that the input image data does not contain four-fold or six-fold rotation points. The sums of squared residuals for the models that have been symmetrized to $plg1$ and $pllg$, are, on the other hand, in our example rather low so that it seems possible that the corresponding symmetrized models of the input image data could combine with the $p2$ symmetrized model to the model with plane symmetry $p2gg$. As long as inequality (9a) is fulfilled for all three cases $p2$, $plg1$, and $pllg$, we can “climb up” from all three of the lower symmetric models at the $k_l = 2$ level to the model that has been symmetrized to plane symmetry group $p2gg$ at the $k_m = 4$ level of Fig. 4.

Plane symmetry group $p2gg$ is a maximal subgroup of $p4gm$, so that another test with inequality (9a) needs to be made if a further climbing up in the plane symmetry group hierarchy tree may be permitted. Let us assume this test is negative (as there are no four-fold rotation points in the input image data). The model that features plane symmetry $p2gg$ is then the Kullback-Leibler best model, which allows for the best separation of the structural information in the input image data from the non-information/noise. It was arrived at without an estimate of the prevailing noise level.

A good estimate of the amount of generalized noise can be obtained after the correct crystallographic symmetry classification has been made

$$\hat{\epsilon}_{best}^2 \approx \frac{\hat{J}_{best}}{rN_{best} - n_{best}} \quad (10),$$

where the subscript *best* stands for the Kullback-Leibler best model of the input image data.

³ The comparison of two non-disjoint symmetrized models with respect of their ability to represent the input image data well is based on having an appropriate “relative measure” of their numerical distance to the common translation-averaged-only model in the first place.

Geometric Akaike weights, which are the probabilities that a certain geometric model of the input image data is indeed the K-L best model in a set of geometric models, can then be calculated on the basis of the estimated noise level and the full G-AIC values of the geometric models according to equation (5). This is not done in this paper and the reader is referred to [7,23] for details on how likelihoods of geometric models are transformed into model probabilities. Note that providing geometric Akaike weights is a second route to deriving uncertainty measures for plane symmetry group and projected Laue class classifications, without which crystallographic symmetry measurements are simply incomplete [36].

We now make up another sake of argument scenario. Let us assume that the correct plane symmetry classification is $p2gg$, but that the geometric model of the input image data that was symmetrized to $p4$ features also a rather low sum of squared residuals of the complex Fourier coefficients. Plane symmetry group $p4$ is then identified as Fedorov type pseudosymmetry as it is disjoint from plane symmetry group $p2gg$, which is the highest genuine symmetry.

In a third sake of argument scenario, let us assume that the sum of squared residual of the complex Fourier coefficient of the model that has been symmetrized to plane symmetry group $p4$ is only modestly larger than those for the $p1g1$ and $p11g$ models and, therefore, sufficiently low that one can not only climb up from $p2$, $p1g1$, and $p11g$ to $p2gg$ (and no further beyond), but also from $p2$ to $p4$ (but no further beyond). The image features then a strong Fedorov type pseudosymmetry.

When a $p4$ pseudosymmetry of the Fedorov type in some input image data is very strong, the unit cell in the image will be nearly of the square type. If the $a = b$ lattice parameter condition for a square Bravais lattice type is fulfilled within error bars of their measurements, one speaks of such a $p4$ pseudosymmetry as being simultaneously of the Fedorov type and a metric specialization. Key to this classification is the fact that plane symmetry $p4$ is measurably more severely broken than $p2$, $p1g1$, and $p11g$ in our third sake of the argument scenario.

The $p4$ symmetrized model of the input image data features Laue class 4. For consistency of the plane symmetry classification for our last scenario, the sum of squared residuals of the Fourier coefficient amplitudes for Laue class 4 need to be higher than that for Laue class $2mm$. See first appendix for the hierarchy tree graph of the projected Laue classes. The variables k_m and k_l refer in the context of classifications into 2D Laue classes to the order of the crystallographic 2D point groups on which these classes are based. All of the equations and inequalities above are valid with the modified meaning of k_m and k_l when information theory based classifications into Laue classes are made.

Laue class $2mm$ is the one that is consistent with all three geometric models of the input image data that contain glide lines in our third scenario, which have been identified as genuine symmetries of the input image data. At the center of the amplitude map of the discrete Fourier transform of the input image data, there can, therefore, only be a four-fold rotation pseudosymmetry point superimposed on a genuine two-fold rotation point that is located at the intersection of two mirror lines.

The logic of the preceding theoretical scenarios discussion will become much clearer when actual numbers are used for our series of synthetic images in the following section.

By first calculating the sums of squared residuals for all eight geometric models of the input image data that feature $k = 2$ and 3, we made sure we know from which plane symmetry group the climbing up in the hierarchy tree of plane symmetry groups, Fig. 4, shall proceed as long as permitted by the fulfillment of inequality (9a).

The sums of squared residuals of the complex structure-bearing Fourier coefficients of the geometric models of the input image data that have been symmetrized to higher symmetric plane symmetry groups are calculated on an as needed basis. Note that the whole procedure can be programmed and does not require visual inspections and comparisons of differently symmetrized version of the input image data. This makes the information theory based classification techniques very different to the other plane symmetry classification methods that are used in electron crystallography [12-19].

Note that to conclude that a certain minimal supergroup is the plane symmetry that minimizes the G-AIC value (and the expected K-L divergence), inequality (9a) has to be fulfilled for all maximal subgroups (and in turn their maximal subgroups). If that is not the case, that plane symmetry is only a Fedorov type pseudosymmetry as it is broken to a larger extent than the genuine plane symmetry that the hypothetical noise-free version of the input image most likely possesses. The correct crystallographic symmetry classifications of a more or less 2D periodic image are the plane symmetry group and Laue class that minimize the expected K-L divergences and G-AIC values.

IV. OBJECTIVE CRYSTALLOGRAPHIC SYMMETRY CLASSIFICATIONS OF A NOISE-FREE AND TWO RELATED SYNTHETIC IMAGES WITH ADDED NOISE

As already mentioned in the first section of this paper, crystallographic symmetry classifications are done here with both the author's methods and the electron crystallography program CRISP [13-15] using the same *.hka files of the latter program. An appropriately chosen series of these files contains all of the information on the periodic-structure bearing Fourier coefficients of the differently symmetrized geometric models of the input image data that is needed for objective classification into plane symmetry groups and projected Laue classes. In the CRISP program, these files are internally used to calculate sets of amplitude and phase angle residuals of the symmetrized input image data as well as ratios of odd to even amplitudes where those are meaningful, i.e. quantifiers of the deviation of a tested plane symmetry group in reciprocal space from the Fourier filtered input image data. These files are also used internally to create symmetrized direct space versions of the input image data by Fourier back transforming for visual comparisons by the CRISP program's user.

The *.hka files can be interactively edited in CRISP. This allows for restrictions of the geometric models of the input image to a desired dynamic range of the Fourier coefficient amplitudes. The program's default value for

this dynamic range is 200. (The maximal dynamic range is 10,000.)

Calculating the discrete Fourier transform with CRISP in its maximal dynamic range setting resulted in 3,666 complex structure-bearing Fourier coefficients for the translation averaged model of the crystallographic pattern in Fig. 1. The pattern in Fig. 2 is, on the other hand, restricted to the back-transform of 956 complex Fourier coefficients.

Lowering the dynamic range leads to a reduction of the number of complex structure-bearing Fourier coefficients of the geometric models and we will make use of that for both the noise-free image and the modest amount of added noise image in the analyzed series, see Figs. 1 and 4.

A limited dynamic range of the Fourier coefficient amplitudes leads unavoidably to a reduction in the accuracy of the geometric models of the input image data. As the direct visual comparison of the crystallographic patterns in Figs. 1 and 2 suggests, this is not a problem in the present study. Limiting the dynamic range has, on the other hand, the benefit of reducing “Fourier ripples” around features with very strong contrast changes, as can be seen in Fig. 2.

With a very large number of data points in the discrete Fourier transform of some input image data with very small amplitudes, one has to wonder if the accuracies of geometric models of the input image data are not compromised by the limited representation length of real numbers in a computer program, accumulated rounding errors, and numerical approximations in the calculation of the discrete Fourier transform.

The CRISP program allows also for restrictions of the spatial resolution of the geometric models of the input image data. This is often necessary for noisy images that are to be classified and will be done here as well for both of the noisy images, Figs. 4 and 5. What will be called “spread noise” below is particularly effective in reducing the number of well resolved data points in a discrete Fourier transform, as demonstrated in [23].

The Matlab script *hkaAICnorm* [23], as written by a graduate student of this author, was used for the extraction of the pertinent information from the exported *.hka files. That script can be freely downloaded and calculates the sums of squared residuals, equations (1) and (2), for all of the geometric models that are used in this study from a series of a *.hka files from the CRISP program.

The noise-free pattern, Fig. 1, of the synthetic image series is classified with respect to its plane symmetry group and projected Laue class in the first subsection below. The second subsection presents the classifications of the two noisy images, Figs. 4 and 5, of the series.

The results of the crystallographic processing of the two noisy patterns of the analyzed series are given in the third subsection. A consequence of the misinterpretation of Fedorov type pseudosymmetries as genuine in the case of the image to which a large amount of approximately Gaussian distributed noise was added is rendered visible there by displaying approximately 1.5 unit cells of both of the crystallographically processed noisy images as Figs. 6 and 7.

A. Classification of the noise-free patterns in the series

Table I lists the sums of squared residuals for a judicious selection of geometric models of the noise-free pattern, of which a small section is shown in Fig. 1. In all three analyses of this paper, circular area selections with a radius of 512 pixels were made in direct space for the calculation of the discrete Fourier transforms. (Circular area selections were shown to deliver better results in [23].) These sections contained approximately 88 primitive unit cells of the crystallographic patterns that are to be classified.

No spatial restriction was made in Fourier space for the calculation of the entries in Table I. The dynamic range of the Fourier coefficient amplitudes was set to 100 in order to restrict the number of data points N in equation, (1), (2), and (5) to something that is easier managed.

Table I: Results of the *hkaAICnorm* MatLab script on the noise-free pattern that underlies Fig. 1 for geometric model selection by inequality (9a).

Plane symmetry group to which the image data have been symmetrized	Sums of squared residuals of complex Fourier coefficients	Sums of squared residuals of Fourier coefficient amplitudes	Number of Fourier coefficients in the geometric model of the image data
<i>p2</i>	0.0042	None	956
<i>p1m1</i>	1.8799	0.0052	937
<i>p11m</i>	1.8642	0.0052	937
<i>p1g1</i>	0.0094	0.0052	934
<i>p11g</i>	0.0081	0.0052	934
<i>c1m1</i>	0.0103	0.0053	924
<i>c11m</i>	0.010	0.0053	924
<i>p3</i>	2.5290	1.3339	954
<i>p2gg</i>	0.0096	0.0052	931
<i>c2mm</i>	0.019	0.0053	924
<i>p4</i>	0.0065	0.0021	948
<i>p4mm</i>	1.9558	0.0063	918
<i>p4gm</i>	0.0102	0.0061	912

Note that the first seven entries in this table consist of the geometric models of the input data that feature two non-translational symmetry operations, whereas the 8th entry features three such operations. All of these eight models are disjoint from each other as there a no connecting vectors between them in the plane symmetry hierarchy tree graph in Fig. 4.

The subsequent three entries in Table I consist of geometric models that feature four non-translational symmetry operations. The last two entries feature eight such operations and the two corresponding models are disjoint from each other (in the translationengleiche sense).

The lowest sum of squared residuals of the complex Fourier coefficients is for the crystallographic pattern that underlies Fig. 1 obtained for the geometric model that has been symmetrized to plane symmetry group *p2*. The model with plane symmetry group *p4* is listed as the one that has the lowest (non-zero) sum of residuals of the amplitudes of the Fourier coefficients.

The symmetry in the amplitude map (projected Laue class) is for the *p4* symmetry model that of point group 4. For easy reference, the entries for geometric models with plane symmetry group *p2* and *p4* are marked in Table I by the shading of the respective two rows.

Geometric models of the input image data with low (but not the lowest) sums of squared complex Fourier

coefficient residual and two or three non-translational symmetry operations may either reveal a genuine symmetry or a Fedorov type pseudosymmetry. What they turn out to actually be depends on the ratios of the sums of squared residuals (and G-AIC values) of these models with respect to those of their minimal supergroups. The selection of entries in Table I has been made in order to demonstrate the climbing up from a lower level of the hierarchy of plane symmetry groups, see Fig. 4, to the next higher level.

The tests if such a climbing up is allowed by the fulfillment of inequality (9a) start always at the geometric model with the plane symmetry that has the lowest sum of squared residuals of the complex Fourier coefficients amongst the mutually disjoint models with two and three non-translational symmetry operations. That starting model features always per definition a genuine symmetry, but more genuine symmetries can potentially be identified by the fulfillment of inequality (9a) for some of its non-disjoint models that may combine with the first identified genuine symmetry to some higher level genuine symmetry.

As already mentioned above, the geometric model that was symmetrized to plane symmetry group $p2$ features the lowest squared residual of the complex Fourier coefficients in Table I. All symmetry models that are candidates for climbing up from the geometric model that was symmetrized to $p2$ in the plane symmetry group hierarchy graph, Fig. 4, i.e. $p2mm$, $p2gm$, $p2mg$, $c2mm$, and $p4$ need to have a sufficiently small sum of squared residuals (and G-AIC values) with respect to all of their maximal subgroups in order to be declared genuine. Otherwise they are Fedorov type pseudosymmetries by definition.

Plane symmetry group $p4$ has only one maximal subgroup, i.e. $p2$, so that only one inequality fulfillment test is needed to find out if the former is a genuine symmetry of the crystallographic pattern in the input image data or not.

For each of the other four models mentioned in the penultimate paragraph, one would need to complete three inequality fulfillment tests. It is, however, already quite clear from the entries in Table I that only the models that were symmetrized to plane symmetry groups $plgl$, $pllg$, $clml$, and $c1lm$, have reasonably low sums of squared residuals (and G-AIC values) to make them reasonable candidates for climbing up tests. The geometric models that were symmetrized to $p2mm$, $p2gm$, and $p2mg$ are just too far from fulfilling inequality (9a) as their sums of squared residuals in Table I are very much larger than that for the $p2$ model.

Table II gives the ratios of the sums of squared residuals of the complex Fourier coefficients for the non-disjoint models of Table I (left hand side of inequality (9a) in the second column) together with the maximal value that these ratios may have (right hand side of inequality (9a) in the third column) in the context of minimization of the G-AIC value of the higher symmetric model of a pair of non-disjoint geometric models of the input image data. The tests if climbing up to the next level of the plane symmetry hierarchy tree is allowed consist of a simple comparison of the numerical values in the second and third column of Table II, which is recorded in the fourth column.

There is only one unconditional “yes” in the fourth column of this table, as marked by the shading of the corresponding row, so that the conclusion has to be drawn that the geometric model which has been symmetrized to plane symmetry group $p4$ features the only other genuine symmetry in the crystallographic pattern that underlies Fig. 1, i.e. the noise-free image of the series.

It is very important to note again that all genuine symmetries above the $k = 2$ and 3 level must by definition be anchored on the least broken plane symmetry group, i.e. the one with the lowest sum of squared residuals for the complex structure-bearing Fourier coefficients at the $k_l = 2$ and 3 levels in Fig. 4. The fulfillment of inequality (9a) for a pair of non-disjoint geometric models that does not fulfill this overwriting requirement can per definition only signify a strong Fedorov type pseudosymmetry, which will be clearly visible in a direct space image. Plane symmetry groups $p2gg$ and $c2mm$ must be Fedorov type pseudosymmetries of the pattern in Fig. 1 because climbing up from $p2$ is not permitted, see first entry in Table II.

Table II: Numerical values of ratios of sums of squared residuals of the complex Fourier coefficients of non-disjoint models of the noise-free pattern that are either within their maximal allowance or not.

	Left hand side of (9a)	Right hand side of (9a)	Inequality (9a) fulfilled?
$p2gg$ over $p2$	2.285714	2.0261506	no, blocking ascent
$p2gg$ over $plgl$	1.021277	2.0032312	yes, but due to pseudosymmetry
$p2gg$ over $pllg$	1.185185	2.0032312	yes, but due to pseudosymmetry
$c2mm$ over $p2$	2.833333	2.0	no, blocking ascent
$c2mm$ over $clml$	1.155340	2.0	yes, but due to pseudosymmetry
$c2mm$ over $c1lm$	1.081818	2.0	yes, but due to pseudosymmetry
$p4$ over $p2$	1.547619	2.008368	yes
$p4mm$ over $p4$	300.8923	1.3438819	no, blocking ascent
$p4gm$ over $p4$	1.569231	1.3459916	no, blocking ascent
$p4gm$ over $p2gg$	1.06250	1.3401361	yes, but due to pseudosymmetry
$p4gm$ over $c2mm$	0.857143	1.3376623	yes, but due to pseudosymmetry

Note that climbing up tests for strong Fedorov type pseudosymmetries to the $k_m = 4$ level, i.e. $p2gg$ and $c2mm$, and up to $k_m = 8$, i.e. $p4gm$, have rather low values for the left hand side of inequality (9a) in Table II. This is due to the corresponding sums of squared complex Fourier coefficient residuals for the matching $k_l = 2$ and 4 levels being comparatively large in Table I. The ratios of such sums may for strong Fedorov pseudosymmetries even fall below unity, as shown for the last entry in Table II.

Ideally, one would base all calculations on symmetrized models of the input image data that feature exactly the same appropriately indexed Fourier coefficients and number of such coefficients. To obtain the same number of data points (complex Fourier coefficients) in all geometric models of the input image data, one would need to treat Fourier coefficients that are absent in certain geometric models as featuring zero amplitude and arbitrary phase. The absences can either be systematic or incidental. In both cases the zero amplitude Fourier coefficients are characteristics of the properly symmetrized geometric

models of the input image data. The smallest possible entry in the second column of Table II should for genuine symmetries then be restricted to unity (in the absence of generalized noise including small calculation errors) and one can also give confidence levels for the classification into genuine symmetries by using equations (A-1) to (A-4) and provide a complete [36] crystallographic symmetry measurement result.

Relying on the *.hka files of CRISP in this study without further editing, this is, however, almost impossible to achieve in practice. The geometric models that are represented by *.hka files with different numbers of data points, different dynamic ranges, and different spatial resolutions do not necessarily give always the best possible symmetrized version of the input image data in Fourier space. For the purpose of the demonstrations in this paper and to allow for the comparison of classification results that were obtained with the information theory based methods to those of the CRISP program, the accuracy of all geometric models is deemed to be more than sufficient.

On all accounts, the geometric models that CRISP provides in the form of exportable *.hka files are always quite representative of symmetrized versions of analyzed images as demonstrated by the successes of numerous electron crystallography studies [13-15] in spite of necessarily different choices for the dynamic range, spatial resolution, and numbers of included Fourier coefficients.

The identification of the projected Laue class that minimizes the expected Kullback-Leibler divergence for the crystallographic pattern that underlies Fig. 1 proceeds analogously. Laue class 4 has already been identified as the point symmetry of the amplitude map of the geometric model that has been symmetrized to plane symmetry group $p4$. Both this projected Laue class and 2D Laue class $2mm$ feature four point symmetry operations, $k_l = 4$, and are disjoint from each other, see hierarchy graph in Fig. A-1.

Table III gives the ratios of the sums of the squared Fourier coefficient amplitude residuals for the non-disjoint models of Table I (with $k_l = 4$) together with the maximal value that these ratios may have for a climbing up to the $k_m = 8$ level. Obviously, one cannot climb up from Laue class 4 to the non-disjoint Laue class $4mm$ with $k_m = 8$ (in Fig. A-1), based on the numbers in this table.

Based on the low sums of squared amplitude residuals in Table I, the models for projected Laue classes $2mm$ and $4mm$ reveal pseudosymmetries in the input image data. This is fully consistent with the identified Fedorov type pseudosymmetries at the plane symmetry group level.

Table III: Numerical values of ratio of the sums of squared amplitude residuals of non-disjoint geometric models of the noise free pattern that are either within their maximal allowance or not.

	Left hand side of inequality (9a)	Right hand side of inequality (9a)	Inequality fulfilled?
$4mm$ (in $c2mm$ setting) over 4	3	1.3438819	no, as it should
$4mm$ (in $p2gg$ setting) over 4	2.90476	1.3577236	no, as it should
$4mm$ over $2mm$ (in $p2gg$ setting)	1.2115385	1.3379878	yes, but due to pseudo-symmetry
$4mm$ over $2mm$ (in $c2mm$ setting)	1.1886792	1.3246592	yes, but due to pseudo-symmetry

To conclude this subsection: plane symmetry group $p4$ (which contains $p2$ as its only maximal subgroup) and Laue class 4 are identified as both genuine in the crystallographic pattern and crystallographically consistent with each other. The identified Fedorov type pseudosymmetries at the lowest level of the hierarchy tree of plane symmetry groups are $plgl$, $pllg$, $clml$, and $cllm$. These pseudosymmetries combine with each other and the identified genuine symmetries to the pseudosymmetry groups $p2gg$, $c2mm$, and $p4gm$. There is a corresponding $4mm$ pseudosymmetry in the amplitude map of the noise free pattern in Fig. 1, but no $4mm$ pseudo-site symmetry in the direct space unit cell of the input image data since the $plml$ and $pllm$ models of this data feature sums of squared complex Fourier coefficient residuals that are way too large to be considered for climbing up tests in the plane symmetry hierarchy tree graph of Fig. 4.

B. Classification of the two noisy patterns of the series

Figures 4 and 5 show sections of the two synthetic patterns that were obtained by adding approximately Gaussian distributed noise to the synthetic pattern that served as basis of Fig. 1, i.e. the noise-free (144 periodic motif repeats containing) image in the analyzed series of undisturbed and deliberately disturbed crystallographic patterns of this paper. The freeware program GIMP [37] was used to add the noise.

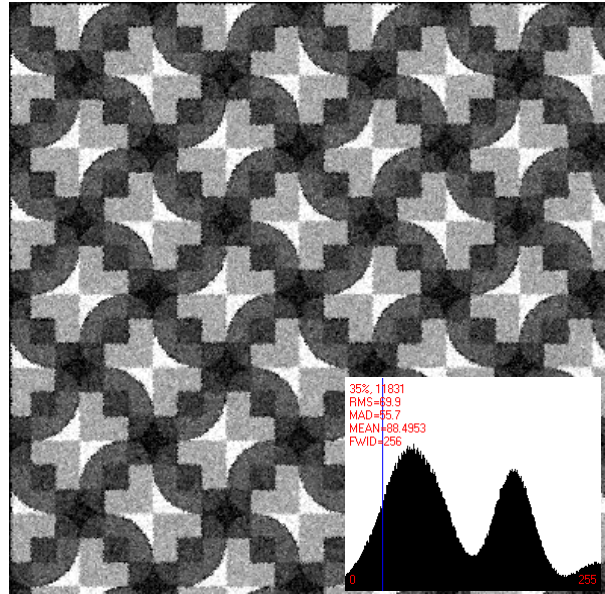


Fig. 5. Section of the underlying crystallographic pattern of Fig. 1 with a moderate amount of approximately Gaussian distributed noise added. The histogram of the whole pattern is provided as inset. The blue thin line and descriptive annotations in red ink in the histogram are provided by the CRISP program.

Spread noise swaps individual pixel intensities in the horizontal and vertical directions by a selected number of pixels. Strictly Gaussian distributed noise only changes the individual pixel values but not their positions in the translation periodic unit cell. The employed mixtures of

strictly Gaussian distributed noise and spread noise add up to approximately Gaussian distributed noise. The strictly Gaussian distributed noise had been added to the crystallographic pattern in Fig. 1 before the spread noise was added with GIMP.

The effects of the added noise are clearly visible in Figs. 4 and 5 and their histogram insets when compared to the histogram inset in Fig. 1. Compared to Fig. 5, there is approximately five times as much added noise in Fig. 6.

This approximate 1 to 5 ratio of the amounts of noise is similar to that of the two noisy synthetic images in [10]. One should, therefore, expect similar crystallographic classification results as in [10], i.e. the correct distinction between genuine symmetries and Fedorov type pseudosymmetries for the image with the moderate amount of noise and a misclassification for the image with the large amount of noise.

We classify the noisy crystallographic pattern in Fig. 5 first. The dynamic range in the employed *.hka file from CRISP was set to 100. The selection in Fourier space was set to a 350 pixel radius (out of 512 pixels), which results in a spatial resolution reduction, that may be appreciated by a comparison of the crystallographically processed version of this image in the third subsection below to the crystallographic pattern in Fig. 1. Both of these settings resulted in a reasonable number of Fourier coefficients in the last column of Table IV.

Table IV: Results of the hkaAICnorm MatLab script on the noise-free image that underlies Fig. 5 for geometric model selection by G-AIC value ratios.

Plane symmetry group to which the image data have been symmetrized	Sums of squared residuals of complex Fourier coefficients	Sums of squared residuals of Fourier coefficient amplitudes	Number of Fourier coefficients in the geometric model of the image data
<i>p2</i>	0.0041	None	665
<i>p1m1</i>	1.7207	0.0041	654
<i>p1lm</i>	1.7210	0.0041	654
<i>p1gl</i>	0.0059	0.0041	652
<i>p1lg</i>	0.0066	0.0041	652
<i>c1m1</i>	0.0081	0.0043	655
<i>c1lm</i>	0.0081	0.0043	655
<i>p3</i>	2.0554	1.3052	685
<i>p2gg</i>	0.0066	0.0041	650
<i>c2mm</i>	0.0102	0.0043	655
<i>p4</i>	0.0040	0.0015	648
<i>p4mm</i>	1.7934	0.0050	644
<i>p4gm</i>	0.0074	0.0050	640

The geometric model with plane symmetry group *p2* features again the lowest sum of squared residuals of the complex Fourier coefficients in this table. Also as before, the model that was symmetrized to plane symmetry group *p4* features the lowest sum of Fourier coefficient amplitude residuals. Again, the rows for these two geometric models are highlighted in Table IV for easy reference by shading.

Analogous to Table II, Table V gives the ratios of the sums of the squared residuals of the complex Fourier coefficients for climbing up tests. There is again only one unconditional “yes” in Table V, as marked by the shading of the row of the corresponding entry, so that the conclusion has again to be drawn that the geometric model which has been symmetrized to plane symmetry group *p4*

features the only other genuine symmetry in the crystallographic pattern that underlies Fig. 5, i.e. the moderate amount of noise added image of the series.

Note that the ratio of the sums of squared residuals of the complex Fourier coefficients is for the “*p4* over *p2*” row of Table V slightly smaller than unity. This is probably the result of both small accumulated calculation errors in the analysis and slight differences in the accuracy of the representation of the geometric models in the employed *.hka files from CRISP.

Table VI is analogous to Table III and lists the ratios of the squared Fourier coefficient amplitude residuals for the modest amount of added noise image. The conclusion from this table is that Laue class 4 describes the symmetry in the amplitude map of the discrete Fourier transform of the crystallographic pattern that underlies Fig. 5. The added approximately Gaussian distributed noise presented no challenge to the image classification task with respect to its crystallographic symmetries when the amount of added noise was modest.

Table V: Numerical values of ratios of sums of squared residuals of the complex Fourier coefficients of non-disjoint models of the pattern with a moderate amount of added noise that are either within their maximal allowance or not.

	Left hand side of (9a)	Right hand side of (9a)	Inequality fulfilled?
<i>p2gg</i> over <i>p2</i>	1.6097561	2.0225564	yes, but due to pseudosymmetry
<i>p2gg</i> over <i>p1gl</i>	1.186441	2.0030675	yes, but due to pseudosymmetry
<i>p2gg</i> over <i>p1lg</i>	1.0	2.0030675	yes, but due to pseudosymmetry
<i>c2mm</i> over <i>p2</i>	2.4878049	2.0	no, blocking ascent
<i>c2mm</i> over <i>c1m1</i>	1.2592593	2.0	yes, but due to pseudosymmetry
<i>c2mm</i> over <i>c1m1</i>	1.2592593	2.0	yes, but due to pseudosymmetry
<i>p4</i> over <i>p2</i>	0.9756098	2.0255639	yes
<i>p4mm</i> over <i>p4</i>	448.35	1.3353909	no, blocking ascent
<i>p4gm</i> over <i>p4</i>	1.85	1.3374486	no, blocking ascent
<i>p4gm</i> over <i>p2gg</i>	1.1212121	1.3384615	yes, but due to pseudosymmetry
<i>p4gm</i> over <i>c2mm</i>	0.7254902	1.3409669	yes, but due to pseudosymmetry

Table VI: Numerical values of ratio of the sums of squared amplitude residuals of non-disjoint models of the moderate amount of added noise pattern that are either within their maximal allowance or not.

	Left hand side of inequality (9a)	Right hand side of inequality (9a)	Inequality fulfilled?
<i>4mm</i> (in <i>c2mm</i> setting) over 4	3.333333	1.3353909	no, as it should
<i>4mm</i> (in <i>p2gg</i> setting) over 4	3.333333	1.3374486	no, as it should
<i>4mm</i> over <i>2mm</i> (in <i>p2gg</i> setting)	1.2195122	1.3384615	yes, but due to pseudo-symmetry
<i>4mm</i> over <i>2mm</i> (in <i>c2mm</i> setting)	1.1627907	1.3389313	yes, but due to pseudo-symmetry

The identified Fedorov type pseudosymmetries at the lowest level are *p1gl*, *p1lg*, *c1m1*, *c1lm*, and *p2gg* (in

noticeable difference to the pseudosymmetries in Fig. 1). These pseudosymmetries combine with each other and the genuine $p2$ and $p4$ symmetries to pseudosymmetry groups $c2mm$ and $p4gm$.

There is again a $4mm$ pseudosymmetry in the amplitude map of the noisy pattern in Fig. 5, but no $4mm$ pseudo-site symmetry in the direct space unit cell of that figure. Clear distinctions between genuine symmetries and Fedorov type pseudosymmetries were, thus, again obtained.

For the synthetic pattern with the large amount of added noise, Fig. 6, the accuracy of the crystallographic symmetry classification with the information theory based methods should be somewhat compromised. As we will see below, this is indeed the case.

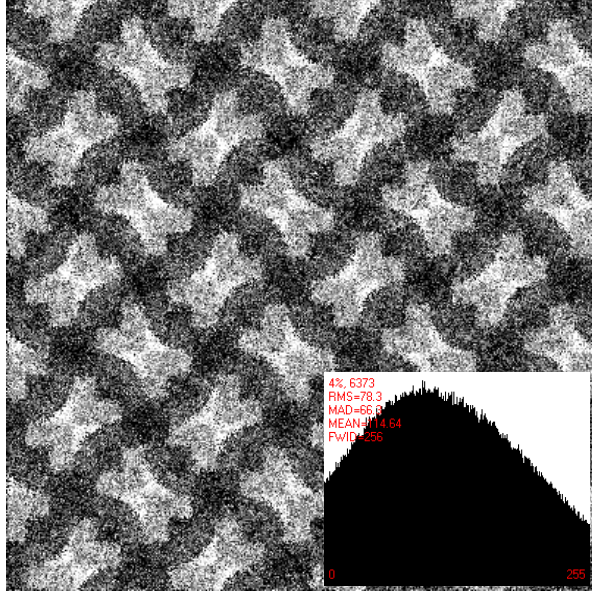


Fig. 6. Section of the underlying crystallographic pattern of Fig. 1 with a large amount of approximately Gaussian distributed noise added. The histogram of the whole pattern is provided as inset. The descriptive annotations in red ink in the histogram are provided by the CRISP program.

The dynamic range of the amplitudes of the Fourier coefficients of the crystallographic pattern in Fig. 6 was for the analysis increased to 200 and the radius of the circular area restricted to 200 pixels because several Fourier coefficients were essentially “washed out” by the large spread noise component of the added noise. These settings ensured that the geometric models of this pattern are represented in Fourier space by a reasonable number of data points in the forth column of Table VII so that the other numbers in that table are on the same order of magnitude as in Tables I and IV.

Table VII gives (in analogy to Tables I and IV) the characteristics of the geometric models for the rather noisy crystallographic pattern that underlies Fig. 6. All of the sums of squared residuals except those for $p1m1$, $p11m$, $p3$, and $p4mm$ are highlighted in this table by shading of the respective rows. This is because, as Table VIII shows, genuine symmetries at the plane symmetry group level can no longer be distinguished from Fedorov type pseudosymmetries as the result of the large amount of added noise.

Plane symmetry group $p4gm$ is now misidentified as genuine and the symmetry that most likely underlies the rather noisy crystallographic pattern in Fig. 6. Note that climbing ups in the plane symmetry hierarchy tree graph of Fig. 4 are now permitted all the way up to the top of the $p4gm$ branch since inequality (9a) is fulfilled for all of the relevant non-disjoint geometric models of the input image data.

It is interesting to check if this misclassification is consistent with the classification of the rather noisy pattern into the most likely projected Laue class as well. Table IX provides the basis for checking this out. Laue class 4 is, however, still identified by inequality (9a) as the one that minimizes the expected Kullback-Leibler divergence. This might be due to 2D Laue class determinations being somewhat less susceptible to added noise.

Table VII: Results of the hkaICnorm MatLab script on the pattern with a large amount of added noise that underlies Fig. 6 for geometric model selection by G-AIC value ratios.

Plane symmetry group to which the image data have been symmetrized	Sums of squared residuals of complex Fourier coefficients	Sums of squared residuals of Fourier coefficient amplitudes	Number of Fourier coefficients in the geometric model of the image data
$p2$	0.0061	None	275
$p1m1$	1.5353	0.0039	271
$p11m$	1.5320	0.0039	271
$p1g1$	0.0069	0.0039	265
$p11g$	0.0078	0.0039	270
$c1m1$	0.0085	0.0041	269
$c11m$	0.0074	0.0041	269
$p3$	1.7565	1.2029	306
$p2gg$	0.0098	0.0039	264
$c2mm$	0.0115	0.0041	269
$p4$	0.0088	0.0028	276
$p4mm$	1.5876	0.0053	276
$p4gm$	0.0109	0.0051	266

Table VIII: Numerical values of ratios of sums of squared residuals of the complex Fourier coefficients of non-disjoint geometric models of the pattern with a large amount of added noise.

	Left hand side of (9a)	Right hand side of (9a)	Inequality fulfilled?
$p2gg$ over $p2$	1.6065574	2.04	yes
$p2gg$ over $p1g1$	1.4202899	2.0037736	yes
$p2gg$ over $p11g$	1.2564103	2.0222222	yes
$c2mm$ over $p2$	1.8852459	2.0218182	yes
$c2mm$ over $c1m1$	1.3529412	2.0	yes
$c2mm$ over $c11m$	1.5540541	2.0	yes
$p4$ over $p2$	1.442623	1.9963636	yes
$p4mm$ over $p4$	180.4091	1.3333333	no, blocking ascent
$p4gm$ over $p4$	1.2386364	1.3454106	yes
$p4gm$ over $p2gg$	1.1122449	1.3308081	yes
$p4gm$ over $c2mm$	0.947826	1.3370508	yes

Also there are many more calculations going into crystallographic symmetry classifications with respect to

plane symmetry groups as compared to their counterparts for projected Laue classes. Rounding errors and approximations in the algorithms may therefore accumulate in the calculation for plane symmetry classifications more than for their counterparts for 2D Laue classes.

From the obvious crystallographic inconsistency that plane symmetry group $p4gm$ and Laue class 4 have both been identified as best representations of the rather noisy pattern in Fig. 6, one should, therefore, conclude that the plane symmetry classification is probably too high and Fedorov type pseudosymmetry has been misinterpreted as genuine symmetry.

Table IX: Numerical values of the ratio of the sums of squared amplitude residuals of non-disjoint geometric models of the pattern with a large amount of added noise.

	Left hand side of inequality (9a)	Right hand side of inequality (9a)	Inequality fulfilled?
4mm (in $c2mm$ setting) over 4	1.8928571	1.3333333	no, but it should for consistency
4mm (in $p2gg$ setting) over 4	1.8214286	1.3454106	no, but it should for consistency
4mm over 2mm (in $p2gg$ setting)	1.3076923	1.3370508	yes, as a result of pseudo-symmetry
4mm over 2mm (in $c2mm$ setting)	1.2926829	1.3246592	yes, as a result of pseudo-symmetry

As mentioned above twice, crystallographic symmetry classification results as obtained in this section were to be expected and are in line with those of [10] for another series of synthetic images with and without added noise that feature Fedorov type pseudosymmetries. The conclusion from both studies must be that the information theory based classification methods work very well for small to moderate amounts of noise. Methods that rely on the suppression of higher order terms in equation (3) must, however, fail if there is too much noise in a more or less 2D periodic pattern that is to be classified with respect to its crystallographic symmetries.

The classification failure is for the image in Fig. 6 not “catastrophic” as even when a misclassification is obtained for the most likely underlying plane symmetry group of the noisiest image, most human experts would have made the same misclassification, at least at first sight. Because it is well known that Fedorov type pseudosymmetries are not rare [9] in nature, one needs to be extra careful with the crystallographic processing of very noisy images in order not to misinterpret noise as structural information.

In the following subsection, the noisy patterns of Figs. 4 and 5 are symmetrized to the plane symmetry groups that our analyses indicated.

C. Results of crystallographic image processing of the two noisy patterns of the analyzed image series

In order to demonstrate the full power of the crystallographic image processing procedure, the classification results of the genuine plane symmetries of the noisy patterns in Fig. 5 and 5 are now used to boost the signal to noise ratio in the noisy crystallographic patterns.

Figure 6 shows approximately 1.5 unit cells of the $p4$ symmetrized pattern of Fig. 5. The conspicuous white bow ties still feature site symmetry 2, as they did in Figs. 1 and 2. Note how much of the added noise has been removed by the crystallographic image processing by a visual comparison between the patterns in Figs. 4 and 6. This becomes also clear by a direct comparison of the histogram insets of both figures.

Very small artifacts of the crystallographic image processing are marked in Fig. 7 by white arrows. There appeared very narrow “straight-quadratic crosses” as artifact of the crystallographic processing that is not part of the original pattern, Fig. 1. Note also that the overall contrast in Fig. 7 is lower than in Fig. 1. These undesirable features are, however, small prices to pay in the opinion of the author for a significant reduction in the noise level by means of the crystallographic processing of a noisy image.

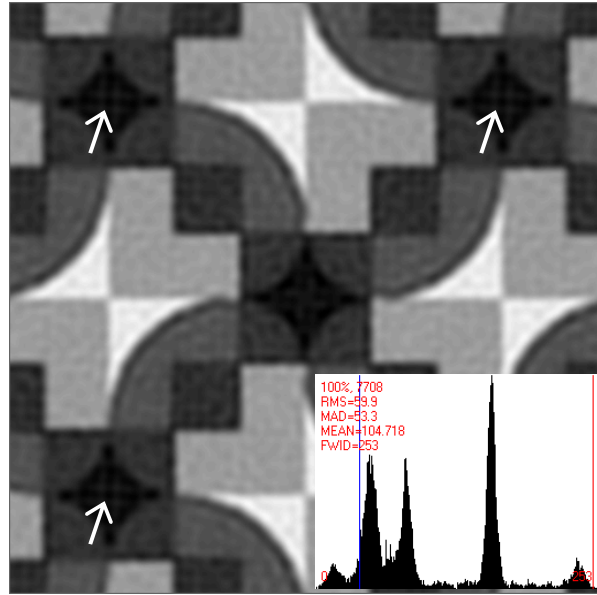


Fig. 7. Approximately 1.5 unit cells of the moderately noisy pattern of Fig. 5 after crystallographic image processing with histogram as inset. The blue and red thin lines and descriptive annotations in red ink in the histogram are provided by the CRISP program. Note the reduction in contrast and spatial resolution with respect to the image in Fig. 1.

Essentially the same can be said about the crystallographically processed version of the very noisy pattern in Fig. 6. The contrast in the crystallographically processed version of this pattern in Fig. 8 is even lower, but conspicuous artifacts of the processing are not visible. This is a consequence of using a smaller number of symmetrized complex Fourier coefficients for the transformation back into direct space. The dark rounded diamonds from Figs. 1, 2, and 6, have now, however, nearly disappeared by blending into the dark surrounding squares. This can also be appreciated by considering the histogram that is inset into Fig. 8.

Because plane symmetry group $p4gm$ has been enforced on the very noisy image in Fig. 6, strong Fedorov pseudosymmetries have been rendered visibly indistinguishable from genuine symmetries in direct space. The conspicuous bow ties feature in Fig. 8, therefore, point symmetry $2mm$, although the corresponding site symmetry in the undisturbed crystallographic pattern was at best

point group 2, as most clearly visible in Fig. 2. Noise in the image has, thus, been misinterpreted as structure as part of the crystallographic image processing.

The increased narrowness of the peaks in the histogram inset of Fig. 8 with respect to their counterparts in the histogram inset of Fig. 7 is due to averaging over twice as many (wrongly identified) asymmetric units in the process of the crystallographic image processing. This averaging created sites in the unit cells that feature now point symmetry group $2mm$ at the fractional unit cell coordinates $\frac{1}{2}, 0, \frac{1}{2}, \frac{1}{2}, 1$, and $1, \frac{1}{2}$, compare to Fig. 2.

Nevertheless, the suppression of the noise in both of the noisy patterns is quite impressive when judged from the histogram insets in Figs. 4 and 5. Again, scanning probe microscopists should take notice of this fact as crystallographic image processing on the basis of objective crystallographic symmetry classifications is now available to them as well. They need, however, to be wary of Fedorov type pseudosymmetries that are easily misinterpreted as genuine symmetries when noise levels are high.

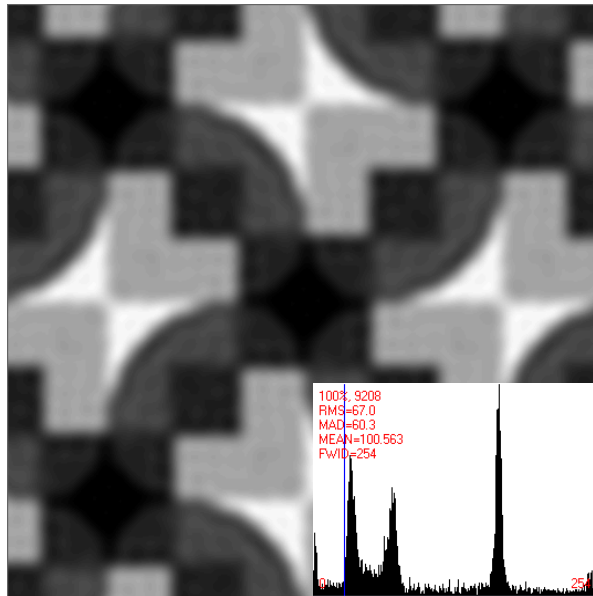


Fig. 8. Approximately 1.5 unit cells of the rather noisy pattern of Fig. 6 after crystallographic image processing with histogram as inset. The blue and red thin lines and descriptive annotations in red ink in the histogram are provided by the CRISP program. Note the reduction in contrast and spatial resolution with respect to both the images in Figs. 1 and 6.

The large amount of added noise pattern, Fig. 6, was crystallographically processed in plane symmetry group $p4gm$, Fig. 8, although the Laue class classification identified a problem with the $p4gm$ classification that is caused by the large amount of added noise. This was done here for the sake of a demonstration of what happens when one symmetrized a more or less 2D periodic pattern to a plane symmetry group that is not crystallographically consistent with the corresponding projected 2D Laue class classification by the information theory based method.

Scanning probe microscopists should heed the advice that noisy images are only to be symmetrized to plane symmetry groups that are crystallographically consistent with the Laue class classification of a more or less 2D periodic image.

V. COMPARISONS OF OUR RESULTS TO SUGGESTIONS BY THE CRISP PROGRAM

The crystallographic symmetry classification results of the previous section are summed up in Table X and are now compared to the results of a traditional classification with the electron crystallography program CRISP, Table XI.

Table X: Plane symmetry and Laue class classifications of the analyzed set of patterns by the author's methods.

Image	Plane symmetry group	Laue class
Free of added noise, Fig. 1	$p4$, with strong $plgl$, $pllg$, $clml$, $cllm$, and somewhat weaker $p2gg$, $c2mm$, $p4gm$ Fedorov type pseudosymmetries	4 , $2mm$ pseudo-symmetry
Moderate amount of added noise, Fig. 5	$p4$, with strong $plgl$, $pllg$, $clml$, $cllm$, $p2gg$, and somewhat weaker $c2mm$, $p4gm$ Fedorov type pseudosymmetries	4 , $2mm$ pseudo-symmetry
Large amount of added noise, Fig. 6	$p4gm$, all Fedorov pseudosymmetries are misclassified as genuine symmetries	4 , $2mm$ pseudo-symmetry

Note that the comparison of the classification results is based on exactly the same structure-bearing Fourier coefficients and their symmetrized versions as facilitated by using the same *.hka files in both types of classifications for the same image area selections.

Table XI: CRISP program suggestions for the plane symmetry classifications of the analyzed series of patterns.

Image	Plane symmetry group
Free of added noise, Fig. 1	$p4gm$
Moderate amount of added noise, Fig. 5	$p2gg$
Large amount of added noise, Fig. 6	$p4gm$

It is clear from Table XI and the results in the previous section that the CRISP suggestions do not make distinctions between genuine symmetries and Fedorov type pseudosymmetries. As mentioned above, most human experts would most likely have classified all three images of the series as belonging to plane symmetry group $p4gm$ (at least at first sight) because it would not occur to them that such distinctions might be necessary although it is well known that Fedorov type pseudosymmetries are not rare in nature [9]. As the analyses in the preceding sections demonstrate, $p4gm$ classifications for the noise-free and large amount of added noise images constitute overestimations of the plane symmetry that is genuinely there, i.e. $p4$, due to the graphic artist's handiwork.

One has to conclude that two of CRISP's three suggestions are about as accurate as most human classifiers would be by visual inspection, at least at first sight. The program's internal thresholds for the interpretation of the CRISP residuals that enabled its plane symmetry estimations must, therefore, be well adjusted. The great popularity of this windows-based computer program with the electron crystallography community is, therefore, well justified. It has been shown elsewhere that the CRISP program is more accurate in the extraction of the lattice parameters of more or less 2D periodic images than two of its competitors [8].

The $p2gg$ classification by CRISP for the modest amount of added noise image, Fig. 5, is consistent with the white bow tie features having a site symmetry that is no higher than point symmetry group 2, as clearly revealed in Fig. 2. It is also consistent with the CRISP derived lattice parameter set of $a = 97.1$ pixels, $b = 97.0$ pixels, and $\gamma = 90.0^\circ$ for the crystallographic pattern in Fig. 5. The difference in the magnitude of the unit vectors is probably not significant based on what has been shown in [8].

As one can interactively test adjacent image areas for their CRISP program suggestions, one can not only assess the accuracy of the program's classification suggestions, but also their precision. It was found that adjacent areas in both the noise-free and moderate amount of noise added image resulted in either $p4gm$ or $p2gg$ classifications with CRISP. The $p4gm$ suggestion by CRISP for the noisiest image did, however, not change with area.

At least the noise-free image in the series should be homogenous so that all adjacent image areas should be classified as featuring the same plane symmetry. One has to note that a large amount of calculations goes into a plane symmetry classification so that the CRISP residuals for different geometric models of the input image data are indeed slightly different for each different area.

The structure-bearing Fourier coefficient amplitude residuals of CRISP do not capture the symmetry of either the projected Laue class or Bravais lattice type of a more or less 2D periodic image, although they are somewhat related to them. No meaningful comparison of the values of the amplitude residual of CRISP to the results in the previous section with respect to projected Laue class classifications can, therefore, be made.

Crystallographic symmetry classifications with the CRISP program rely in practice heavily on visual comparisons between the translation averaged (Fourier filtered) and differently symmetrized versions of the input image data by an expert practitioner of electron crystallography. Faced with a $p2gg$ classification and a 2D Bravais lattice that is almost of the square type by CRISP (as obtained for the moderate amount of added noise image), most electron crystallographers would have simply overwritten that suggestion after visual inspections and concluded that the plane symmetry groups is $p4gm$, based on a square unit cell and discount the possibility of a metric specialization.

Using the author's information theory based methods, no visual comparisons between the translation averaged and differently symmetrized versions of the input image data are necessary. Crystallographic symmetry classifications can, therefore, be made without human supervision, but under the currently necessary assumption that there is indeed more than translation symmetry in a noisy image.

Therefore, the user no longer needs to be an electron crystallographer to employ crystallographic image processing techniques. This fact allows sufficiently well resolved more or less 2D periodic images from a wide range of samples that are recorded with different types of microscopes to be processed crystallographically. Previous successes in the crystallographic processing of images from scanning tunneling and atomic force microscopes are quoted and shown in [24,28].

VI. SUMMARY, CONCLUSIONS, AND OUTLOOK

Information theory based crystallographic symmetry classification methods for plane symmetry groups and projected Laue classes have been demonstrated on a series of three synthetic patterns. The classifications were for the two noisy patterns complemented by the showing of the corresponding images and their histograms before and after their crystallographic processing. Note that these pairs of images needed to be shown in this paper for demonstration purposes, but crystallographic image processing by the new method can proceed without prior visual inspections of such images by human beings.

It is concluded that the information theory based classification methods are statistically sound and superior to all other existing methods, including the visual insights of human expert classifiers as far as their accuracy and precision at first sight is concerned. Information theory based methods should be developed for crystallographic symmetry classifications in three spatial dimensions as there is also subjectivity in the current practice of single crystal X-ray and neutron crystallography.

The assumption had to be made that there is indeed more than translation symmetry in a more or less 2D periodic image. This may, however, not always be the case. There are certainly (approximately) 2D periodic images (with and) without noise in which all point/site symmetries higher than the identify operation are only pseudosymmetries and not genuine.

Those images would be misclassified by the author's methods at the present stage of their development. In order to remedy this shortcoming, one needs to come up with a sum of squared residuals and a G-AIC formalism that captures the deviation of a more or less 2D periodic pattern from its crystallographic translation symmetry in a statistically sound manner.

A method that will allow for binary type discriminations between a quasicrystal and its rational approximants is currently being development by this author on the basis of their projected Laue classes. The detection of noncrystallographic symmetries (as defined in the introduction as being incompatible with translation symmetry) is beyond the scope of the demonstrated methods and there are no plans by this author to try to tackle that kind of problem.

Acknowledgments

The current member of Portland State University's Nano-Crystallography group, Regan Garner, Choomno Moos, Grayson Kolar, Gabriel Eng, Noah Allen, and Luckas von Koch are thanked for critical proofreads of the manuscript. Regan Garner is also thanked for the graphs in Figs. 3 and A-1.

REFERENCES

- [1] M. I. Aroyo (ed.), *International Tables for Crystallography, Volume A, Space-Group Symmetry*, 6th rev. ed., Chichester, UK: Wiley, 2016.
- [2] Th. Hahn (ed.), *International Tables for Crystallography, Brief Teaching Edition of Vol. A Space Group Symmetry*, 5th edition, John Wiley & Sons, Ltd, 2010.

- [3] W. Steurer and S. Deloudi, *Crystallography of Quasicrystals: Concepts, Methods and Structures*, 2009.
- [4] https://dictionary.iucr.org/Noncrystallographic_symmetry.
- [5] https://dictionary.iucr.org/Pseudo_symmetry.
- [6] M. Nespolo, B. Souvignier, and D. B. Litvin, "About the concept and definition of "noncrystallographic symmetry," *Z. Kristallogr.*, vol. 223, pp. 605–606, 2008, doi: 10.1524/zkri.2008.1137.
- [7] P. Moeck, "Towards Generalized Noise-Level Dependent Crystal-lographic Symmetry Classifications of More or Less Periodic Crystal Patterns," *Symmetry*, vol. 10, article 133 (46 pages), 2018, doi: 10.3390/sym10050133.
- [8] P. Moeck and P. DeStefano, "Accurate lattice parameters from 2D-periodic images for subsequent Bravais lattice type assignments," *Adv. Struct. Chem. Imag.*, vol. 4, article 5 (33 pages), 2018, doi: 10.1186/s40679-018-0051-z.
- [9] E. V. Chuprunov, "Fedorov pseudosymmetry of crystals: Review," *Crystallogr. Rep.*, vol. 52, pp. 1–11, 2007, doi: 10.1134/S1063774507010014
- [10] P. Moeck and A. Dempsey, "Crystallographic symmetry classifications of noisy 2D periodic images in the presence of pseudo-symmetries of the Fedorov type," *Microsc. and Microanal.* vol. 25, pp. 1936–1937, 2019, doi: 10.1017/S1431927619010419.
- [11] C. L. Lawson, H. M. Berman, and W. Chiu, "Evolving data standards for cryo-EM structures," *Struct. Dyn.*, vol. 7, paper 014701 (11 pages), 2020, doi: 10.1063/1.5138589.
- [12] J. M. Valpuesta, J. L. Carrascosa, and R. Henderson, "Analysis of Electron Microscope Images and Electron Diffraction Patterns of Thin Crystals of $\text{O}29$ Connectors in Ice," *Journal of Molecular Biology*, vol. 240, pp. 281–287, 1994, doi: 10.1006/jmbi.1994.1445.
- [13] S. Hovmöller, "CRISP: crystallographic image processing on a personal computer," *Ultramicroscopy*, vol. 41, pp.121–135, 1992, doi: 10.1016/0304-3991(92)90102-P.
- [14] X. Zou and S. Hovmöller, "Electron Crystallography: Structure Determination by HREM and Electron Diffraction", in: *Industrial Applications of Electron Microscopy*, Ed. Z. R. Li, Marcel Dekker, New York, pp. 583–614, 2003.
- [15] X. Zou, S. Hovmöller, and P. Oleynikov, *Electron Crystallography: Electron Microscopy and Electron Diffraction*, IUCr Texts on Crystallography No. 16, 2011, Oxford University Press, Oxford, U.K., doi: 10.1093/acprof:oso/9780199580200.001.0001.
- [16] B. Gipson, X. Zeng, Z. Y. Zhang, and H. Stahlberg, "2dx—User-friendly image processing for 2D crystals," *J. Struct. Biol.*, vol. 157, pp. 64–72, 2007, doi: 10.1016/j.jsb.2006.07.020.
- [17] Z. Wan, Y. Liu, Z. Fu, Y. Li, T. Cheng, F. Li, and H. Fan, "Visual computing in electron crystallography," *Zeitschrift für Kristallographie*, vol. 218, pp. 308–315, 2003, doi:10.1524/zkri.218.4.308.20739.
- [18] X.-M. Li, F.-H. Li, and H.-F. Fan, "A revised version of the program VEC (visual computing in electron crystallography)," *Chinese Phys.*, vol. B18, pp. 2459–2463, 2009.
- [19] R. Kilaas, L. D. Marks, and C. S. Own, "EDM 1.0: Electron direct methods," *Ultramicroscopy*, vol. 102, pp. 233–237, 2005, doi: 10.1016/j.ultramicro.2004.10.004, version 2.0.1, <http://www.numis.northwestern.edu/edm/documentation/edm.htm>, and version 3.0 <http://www.numis.northwestern.edu/edm/>.
- [20] Y. Liu, H. Hel-Or, C. S. Kaplan, and L. Van Gool, "Computational symmetry in computer vision and computer graphics", *Foundations and Trends® in Computer Graphics and Vision*, vol. 5, pp. 1–195, 2009, doi: 10.1561/06000000008.
- [21] M. Agustí-Melchor, A. Rodas-Jordá, and J. M. Valiente-González, "Computational symmetry via prototype distances for symmetry groups classification," *Proc. Intern. Conf. Computer Vision Theory and Applications*, 2011, pp. 85–94, doi: 10.5220/0003375300850093.
- [22] F. Albert, J. M. Gómis, J. Blasco, J. M. Valiente, and N. Aleixos, "A new method to analyse mosaics based on symmetry group theory applied to Islamic geometric patterns," *Computer Vision and Image Understanding*, vol. 130, pp. 54–70, 2015, doi: 10.1016/j.cviu.2014.09.002.
- [23] A. Dempsey and P. Moeck, "Objective, probabilistic, and generalized noise level dependent classifications of sets of more or less 2D periodic images into plane symmetry groups," *arXiv: 2009.08539*, (74 pages, Dec. 15, 2020).
- [24] P. Moeck, "Towards more reasonable identifications of the symmetries in noisy digital images from periodic and aperiodic crystals," *Proc. 21st IEEE Intern. Conf. on Nanotech.*, 2021, (4 pages), accepted.
- [25] K. Kanatani, "Comments on "Symmetry as a Continuous Feature"," *IEEE Transactions on Pattern Analysis and Machine Intelligence*, vol. 19, pp. 246–247, 1997, doi: 10.1109/34.584101.
- [26] K. Kanatani, "Geometric information criterion for model selection," *International Journal of Computer Vision*, vol. 26, pp. 171–189, 1998, doi: 10.1023/A:1007948927139.
- [27] K. Kanatani, "Uncertainty modeling and model selection for geometric inference," *IEEE Transactions on Pattern Analysis and Machine Intelligence*, vol. 26, pp. 1307–1319, 2004, doi: 10.1109/TPAMI.2004.93.
- [28] P. Moeck, "Advances in crystallographic image processing for scanning probe microscopy," in: A. Méndez-Villas, (ed.), *Microscopy and Imaging Science: Practical Approaches to Applied Research and Education*, pp. 503–514, 2017, Microscopy Book Series No. 7, Badajoz: FORMATEX Research Center, *arXiv: 2011.13102v2* (12 pages, Nov. 30, 2020).
- [29] D. McLachlan (Jr.), "Crystal structure and information theory," *Proc. Natl. Acad. Sci. USA*, vol. 44, pp. 948–956, 1958, doi: 10.1073/pnas.44.9.948.
- [30] S. Park and C. F. Quate, "Digital filtering of scanning tunneling microscope images", *J. Appl. Phys.*, vol. 62, pp. 312–314, 1987, doi: 10.1063/1.339150.
- [31] L. Jones, H. Yang, T. J. Pennycook, M. S. J. Marshall, S. Van Aert, N. D. Browning, M. R. Castell, and P. D. Nellist, "Smart Align—a new tool for robust non-rigid registration of scanning microscope data," *Adv. Struct. Chem. Imag.*, vol. 1, paper 8 (16 pages), 2015, doi: 10.1186/s40679-015-0008-4.
- [32] P. Moeck, "On classification approaches for crystallographic symmetries of noisy 2D periodic patterns", *IEEE Trans. Nanotech.*, vol. 18, pp. 1166–1173, 2019, doi: 10.1109/TNANO.2019.2946597, expanded version (21 pages) *arXiv: 1902.04155v4*, May 29, 2021.
- [33] E. Knoll, "Life after Escher: A (Young) Artist's Journey," In: Schattschneider D., Emmer M. (eds.), *M. C. Escher's Legacy*. Springer, Berlin, Heidelberg, pp. 189–198, 2003, doi: 10.1007/3-540-28849-X_19.
- [34] Microsoft ICE 2.0, Image Composite Editor, for Windows Vista SP2, 7, 8, and 10.
- [35] H. Burzlaff, W. Fisher, and E. Heller, "Die Gitterkomplexe der Ebenengruppen," *Acta Cryst.*, vol. A24, pp. 57–67, 1968, doi: 10.1107/S0567739468000070 (in German).
- [36] J. R. Helliwell, "Combining X-rays, neutrons and electrons, and NMR, for precision and accuracy in structure–function studies," *Acta Cryst.*, vol. A77, pp. 173–185, 2021, doi: 10.1107/ S205327332100317X.
- [37] GIMP 2.10, for Windows 7 and above, freely downloadable at <https://www.gimp.org/>.

- [38] V. Kopský and D. B. Litvin, *International Tables for Crystallography, Vol. E, Subperiodic groups*, 2nd ed., Chichester, UK: John Wiley & Sons, 2010.
- [39] R. K. Vasudevan, N. Laanait, E. M. Ferragut, K. Wang, D. B. Geohagan, K. Xiao, M. Ziatdinov, S. Jesse, O. Dyck, and S. V. Kalinin, "Mapping mesoscopic phase evolution during e-beam induced transformations via deep learning of atomically resolved images," *npj Comp. Mater.*, vol. 4, article 30 (9 pages), 2018, doi: 10.1038/s41524-018-0086-7.
- [40] J. A. Aguiar, M. L. Gong, R. R. Unocic, T. Tasdizen, and B. D. Miller, "Decoding crystallography from high-resolution electron imaging and diffraction datasets with deep learning," *Sci. Adv.*, vol. 5, article eaaw 1949 (10 pages), 2019, doi: 10.1126/sciadv.aaw1949.
- [41] L. C. O. Tiong, J. Kim, S. S. Han, and D. Kim, "Identification of crystal symmetry from noisy diffraction patterns by a shape analysis and deep learning," *npj Comput. Mater.*, vol. 6, article 196 (11 pages), 2020, doi: 10.1038/s41524-020-00466-5.
- [42] K. Kaufmann, C. Zhu, A. S. Rosengarten, D. Maryanovsky, T. J. Harrington, E. Marin, and K. S. Vecchio, "Crystal symmetry determination in electron diffraction using machine learning," *Science*, vol. 367, pp. 564–568, 2020, doi: 10.1126/science.aay3062, extended preprint "Paradigm shift in electron-based crystallography via machine learning," *arXiv:1902.03682*.
- [43] K. Kaufmann, C. Zhu, A. S. Rosengarten, and K. Vecchio, "Deep Neural Network Enabled Space Group Identification in EBSD," *Microscopy and Microanalysis*, vol. 26, pp. 447–457, 2020, doi: 10.1017/S1431927620001506.
- [44] S. Dash and A. Dasgupta, "Towards a Universal Classifier for Crystallographic Space Groups: A Trickle-Down Approach to Handle Data Imbalance," In: J. Nichols, B. Verastegui, A. Maccabe, O. Hernandez, S. Parete-Koon, and T. Ahearn (eds.), *Communications in Computer and Information Science*, vol. 1315, Springer, 2020, (Smoky Mountain Computational Science and Engineering Conference, MC 2020: Driving Scientific and Engineering Discoveries Through the Convergence of HPC, Big Data and AI), doi: 10.1007/978-3-030-63393-6_31.
- [45] K. Choudhary, K. F. Garrity, C. Camp, S. V. Kalinin, R. Vasudevan, M. Ziatdinov, and F. Tavazza, "Computational scanning tunneling microscope image database", *Scientific Data*, vol. 8, article 57 (9 pages), 2021, doi: 10.1038/s41597-021-00824-y.
- [46] H. Wondratschek and U. Müller, *International Tables for Crystallography, Vol. A1 Symmetry relations between space groups*, 1st edition, Kluwer Academic Publ. 2004.
- [47] T. S. Cohen, and M. Welling, "Group Equivariant Convolutional Networks," *Proc. 33rd International Conference on Machine Learning*, New York, vol. 48, pp. 2990–2999, 2016, doi: 10.5555/3045390.3045705.
- [48] A. Klug, "Image Analysis and Reconstruction in the Electron Microscopy of Biological Macromolecules," *Chem. Scr.*, vol. 14, pp. 245–256, 1978–79.
- [49] S. Hvömmöller, A. Sjögren, G. Farrants, M. Sundberg, and B.-O. Marinder, "Accurate atomic positions from electron microscopy," *Nature*, vol. 311, pp. 238–241, 1984, doi: 10.1038/311238a0.
- [50] O. E. Piro, "Information Theory and the 'Phase Problem' in Crystallography," *Acta Cryst.*, vol. A39, pp. 61–68, 1983, doi: 10.1107/S0108767383000094.
- [51] D. P. Varn and J. P. Crutchfield, "Chaotic crystallography: how the physics of information reveals structural order in materials", *Current Opinion in Chemical Engineering*, vol. 7, pp. 47–56, 2015, doi: 10.1016/j.coche.2014.11.002.

Appendices

Appendix A: Hierarchy tree of the crystallographic 2D point groups that are projected Laue classes

Figure A1 presents the hierarchy tree graph of the crystallographic point groups that are projected Laue classes. The two ordering principles in this graph are the order of the point group/Laue class on the left and right hand side increasing from the bottom to the top and the maximal subgroup and minimal supergroup relationships. The ratios of the sums of squared residuals of the amplitudes of the structure-bearing Fourier coefficients for climbing up tests from a lower level of the hierarchy to a higher level that are permitted by inequality (9b) are also given.

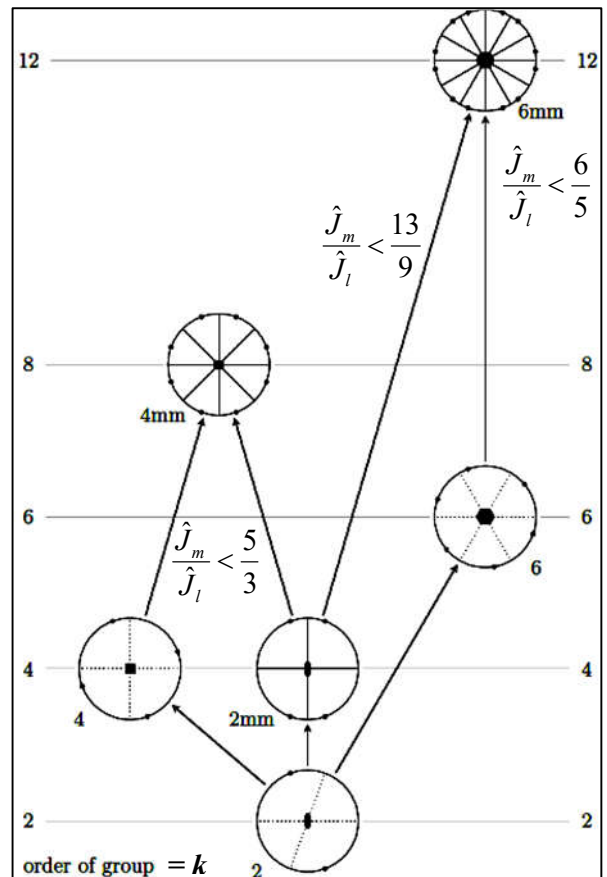


Fig. A-1. Hierarchy tree of the 2D point symmetry groups that are projected Laue classes with ratios of sums of squared Fourier coefficient amplitude residuals as insets. The inset ratios are valid for equal numbers of structure bearing Fourier coefficients of geometric models and apply to transitions from one k_l level of the graph to one of its permitted k_m level. Maximal subgroups are connected to their minimal supergroups by arrows.

Appendix B: Ad hoc confidence levels for classifications into minimal supergroups

Based on Kanatani's information content ratio equation [26], ad hoc defined confidence levels for the model selections in favor of the more symmetric/restricted geometric model can for the special case $N_m = N_l$ be straightforwardly defined. For two non-disjoint geometric models one obtains:

$$K = \sqrt{\frac{1 - \frac{1}{k_l} \left(\frac{\hat{J}_m}{\hat{J}_l} + \frac{2}{1 - \frac{1}{k_l}} \right)}{1 + \frac{1}{k_l} \left(\frac{\hat{J}_m}{\hat{J}_l} + \frac{2}{1 - \frac{1}{k_l}} \right)}} \leq 1 \quad (\text{A-1}),$$

and the critical value for K is obtained for inserting the condition

$$\frac{\hat{J}_m}{\hat{J}_l} = 1 \quad (\text{A-2}),$$

into (A-1) so that

$$K_{critical} = \sqrt{\frac{k_m - \frac{k_m}{k_l} + 2}{k_m + \frac{k_m}{k_l}}} < 1 \quad (\text{A-3})$$

results.

Obviously, $K \geq K_{critical}$ is valid as the ratio of the two sums of squared residuals ranges from unity (A-2) to a constant value that is larger than unity and depends on the particular combination of k_m and k_l in inequality (9b).

When the ratio of the squared residuals is unity (as in equation (A-2)), one has 100 % confidence in choosing the more symmetric model over the less symmetric model. Both models fit the input image data equally well in that special case, which will in practice only be obtained for noise free images, perfect geometric models, and with a perfectly accurate algorithm.

When inequality (9b) is not fulfilled, one has zero confidence in the selection of the more constrained model over its less symmetric counterpart. This is formalized by

$$C_m = \frac{1 - K}{1 - K_{critical}} (100\%) \quad (\text{A-4}),$$

which takes on a value between zero and 100 % as a function of the ratio of the sums of squared residuals.

A ratio of unity for two sums of squared residuals (equation A-2) of two non-disjoint geometric models of some image input data and a 100 % confidence of selecting the higher symmetric model as the better representation of said data will in practice only be obtained with a perfect algorithm and mathematical idealizations of real world images.

Appendix C: Comments on alternative computational symmetry and machine learning approaches

Individual members of the computational symmetry community [20] need to be credited with realizing the importance of Kanatani's geometric form of information theory [25-27] for their field roughly five years earlier than this author did. As mentioned above, this statistical theory deals objectively with symmetry inclusion relations and ensures that the least broken symmetry can be reliably identified in noisy images.

The works of the computational symmetry community are concerned with direct space analyses and often lack crystallographic rigor (such as a display of ignorance about the concepts of standard plane symmetry group origin choices and the importance of site symmetries [1,2]). Maybe this is one of the reasons that only two studies exist, to the best of this author's knowledge, where a G-AIC was used in the classification of a periodic movie, i.e. a time-periodic series of 2D images, in direct space. These two studies ignored the standard origin choices for freeze groups [38] and their results are somewhat questionable, as discussed in appendix E of [7].

The preoccupation of the computational symmetry community with making classifications in direct space is from the perspective of natural scientists and engineers misguided. In science and engineering, one would always use Fourier methods when one is confronted with a problem that is periodic in space or time. When the sequence of periodic repeats is small, one would simply augment it with multiple copies of the original data in order to enable effective space or time translation-averaging by a discrete Fourier transform.

Note that except for the two above mentioned studies of periodic time series, all of the so far reviewed [32] crystallographic symmetry classifications into plane symmetry groups, frieze groups, site/point symmetries, and 2D Bravais lattice types by the computational symmetry community involved internally programmed thresholds for automated interpretations, i.e. subjectivity disguised in computer code in other words.

These classifications are, therefore, all subjective at a fundamental level in spite of having been under development for more than half of a century.

There is also a new breed of materials-data scientist who tries to employ machine learning systems for crystallographic symmetry classifications [39-45] that appear at first sight to be objective. All of their classifications were performed in reciprocal/Fourier space, as this is the most sensible thing to do. The subjectivity rest in machine learning approaches with the selection of the training images.

More or less kinematic diffraction patterns from real crystals and calculated amplitude maps of discrete Fourier transforms from more or less 2D periodic images do not contain enough symmetry information to arrive at unambiguous space group classifications by machine learning systems even when complications due to symmetry inclusion relations are ignored. Note that there are only 11 Laue classes (centrosymmetric crystal classes and point groups) but 230 space groups in three dimensions, projecting to six 2D Laue classes and 17 plane symmetry groups (with 21 settings) [1,2]. Note further that the listing of the maximal subgroups of the space groups takes up over 300 pages in [46]. There are, thus, a lot of symmetry inclusion relations to be considered in 3D.

Structural and symmetry information that has been lost by the recording of the outcome of a crystallographic diffraction experiment or the calculation of Fourier transform amplitudes of a more or less 2D periodic image, i.e. the equivalent of collapsed wave functions, can probably not be recovered by contemporary "correlation detection machines". The goals of the study of [40] are, therefore, way too ambitious.

More structural information than in essentially kinematic electron diffraction patterns is encoded in dynamical convergent beam electron diffraction patterns. One may, however, remain skeptical if that additional amount of structural information may suffice for reliable space group determinations so that "*a universal classifier for crystallographic space groups*" [44] might eventually be created or remain a pipe dream.

Shannon's information theory was used more than 60 years ago to show that complete crystal structure determinations are theoretically possible based on diffraction data alone when *analytic* routes are followed [29]. This author is not aware that something even remotely comparable has been demonstrated with respect to the utility of machine learning systems for crystallographic symmetry classifications and crystal structure determination. Note that compared to a whole crystal structure determination, an accompanying space group classification is much less involved.

One may, therefore wonder where the merit lies at present in attempting to prepare correlation detection machines for classifications that necessarily encounter symmetry inclusion relations when this might well be outside of the present capabilities of machine learning systems. Inclusion relations are, for example, ignored in [47] in connection with a deep convolutional neural network in which point symmetries 4 and $4mm$ are combined with the inherent translation invariance of such machines. That paper states also that “*a strong theory of neural network design is currently lacking*”.

It is well known that pseudosymmetries are not rare in real-world crystals [9]. Images with pseudosymmetries are so far absent from labeled training datasets in machine learning studies [39-45], so that distinctions between genuine symmetries and pseudosymmetries cannot be achieved by such machines. Also, several of these studies did not even include noisy and experimental images into their training data sets. It is too early to review the recent successes and failures of the machine learning approaches with respect to crystallographic symmetry classifications as this was last done by this author in the expanded on-line version of [32] in the year 2019.

As this paper shows, statistically sound analytic alternatives to both the computer codes of the computational symmetry community and the application of machine learning systems to the task of crystallographic image classifications do exist [7,10,23,24,28]. These alternatives even outperform human experts with respect to their accuracy and precision in the admittedly difficult distinction between genuine symmetries and strong Fedorov type pseudosymmetries (as demonstrated in this paper).

As to the merits of *analytical* approaches in general, crystallographers have over the years found multiple workarounds for the recovery of the lost structure factor phases of crystal diffraction experiments. One such workaround is used in electron crystallography, where good estimates of these phases are recovered from sufficiently well resolved images of a crystal (Nobel Prizes to Sir Aaron Klug, 1982, Richard Henderson, Joachim Frank, and Jacques Dubochet, 2017).

These estimates are then used for crystallographic symmetry classifications of 2D projections of space group symmetries and the subsequent crystallographic processing of the images [48], which facilitated the solving of an inorganic crystal structure to atomic resolution by electron microscopy [49] as early as the year 1984. The projected space group was known a priori in [49] so that it did not need to be determined from the input data for the crystallographic processing of the experimental transmission electron microscope images.

The author of [29] concluded more than six decades ago that “*information theory ... points the way to extending the resolution of detail in electron micrographs of crystals*”. Nearly four decades ago, justifications for the validity of the direct methods approach (Nobel Prizes to Herbert A. Hauptman and Jerome Karle, 1985) of diffraction based crystallography have been derived on the basis of Shannon’s information theory [50]. The world had, however, to wait until 1996 for Kanatani’s geometric form of information theory [25-27] and his solution to the symmetry inclusion problem to emerge.

The application of Kanatani’s statistical theory to crystallographic symmetry classifications is by now reasonably well developed so that it can be taken up by the wider scientific community. In other words, there is no good justification to stick to a “*procedure*” that has of the year

2020 been ruled to be “*not sufficiently standardized*” and where “*a number of different variables (e.g. ... threshold value for interpretation) can substantially impact the outcome*” [11]. There is also no good justification to wait for robots to do accurate crystallographic symmetry classifications for us.

A statistical extension of classical (space group based) crystallography has recently been proposed on the basis of Shannon’s information theory [51]. In the humble opinion of this author, the future seems to belong to the *analytical* approaches. The most objective (unbiased) description of a noisy system that is not completely amenable to experimental verification is, after all at any one time, the one with maximum entropy (minimized expected Kullback-Leibler divergence) with respect to whatever has already been well established by science and mathematics.